# ATLAS NOTE

ATLAS-CONF-2011-155

November 13, 2011


# Search for supersymmetry with jets and missing transverse momentum: Additional model interpretations

ATLAS Collaboration

**Abstract**

This note describes a set of new model interpretations of the search for supersymmetry using final states with jets and missing transverse momentum. Limits are presented for Minimal Supersymmetric Standard Model scenarios with only squark and gluino production and decays for different masses of the lightest supersymmetric particle (LSP), and in a model of Minimal Universal Extra Dimensions (MUED). At the 95% confidence level, gluino (squark) masses below 700 (650) GeV are excluded for LSP masses up to 200 GeV assuming direct decays, with the squark (gluino) mass set to 4.5 TeV. Equal-mass squarks and gluinos are excluded below 1025 GeV for LSP masses up to 400 GeV. Less stringent limits are set on gluino production with a single step cascade decay via a chargino. Analogous single-step squark decays are not bounded when the nominal production cross sections and branching fractions are assumed. In a MUED model with one extra dimension, a bound of 600 GeV is set on the compactification scale $R^{-1}$, for values of the compression scale $\Lambda \cdot R$ between 2 and 40, translating to a lower bound of 730 GeV on the mass of the Kaluza-Klein gluon. These are the most stringent constraints on MUED from direct collider searches.



# 1 Introduction

Recently, the ATLAS Collaboration has published a search for supersymmetry (SUSY) in final states with jets and missing transverse momentum in proton-proton ($pp$) collisions at centre-of-mass energy $\sqrt{s} = 7$ TeV using a data set corresponding to an integrated luminosity of 1.04 fb$^{-1}$ [1]. In five different signal regions, no excesses above the Standard Model (SM) prediction were observed, and limits were set on gluino and first- and second-generation squark masses in the Minimal Supersymmetric Standard Model (MSSM), assuming the lightest supersymmetric particle (LSP) to be massless, as well as on parameters of the Constrained MSSM/Minimal Supergravity (CMSSM/MSUGRA) framework.

This note describes a set of further interpretations of this search, in terms of simplified models with well-defined gluino or squark production and decay modes, where the neutralino LSP is massive, and in terms of a Minimal Universal Extra Dimensions (MUED) model .

# 2 Analysis

The results in this note are fully derived from the data set and the analysis described in Ref. [1]. For convenience, a short summary of the analysis is given here.

The data used in this analysis were collected in the first half of 2011 with the LHC operating at $\sqrt{s} = 7$ TeV. The main trigger required events to contain a leading jet with a transverse momentum ($p_{\mathrm{T}}$), measured at the electromagnetic scale, above 75 GeV and missing transverse momentum above 45 GeV.

Jet candidates are reconstructed from calorimeter clusters [2] using the anti-$k_t$ jet clustering algorithm [3] with a distance parameter of 0.4 and calibrated as detailed in Ref. [4]. They are required to satisfy transverse momentum and pseudorapidity ($\eta$) cuts of $p_{\mathrm{T}} > 20$ GeV and $|\eta| < 2.8$ to count towards the signal selection. Additionally, jets with $p_{\mathrm{T}} > 20$ GeV and $2.8 < |\eta| < 4.5$ contribute towards the computation of the missing transverse momentum. Electron candidates are required to have $p_{\mathrm{T}} > 20$ GeV, have $|\eta| < 2.47$, and pass the 'medium' shower shape and track selection criteria of Ref. [5]. Muon candidates [5] are required to have $p_{\mathrm{T}} > 10$ GeV and $|\eta| < 2.4$. An overlap removal procedure resolves ambiguities between electrons, muons and jets that are close in $\Delta R = \sqrt{(\Delta\eta)^2 + (\Delta\phi)^2}$, where $\Delta\phi$ is the difference in the azimuthal angles of the two objects.

The measurement of the missing transverse momentum two-dimensional vector $\vec{P}_{\mathrm{T}}^{\,\mathrm{miss}}$ (and its magnitude $E_{\mathrm{T}}^{\mathrm{miss}}$) is then based on the transverse momenta of all electron and muon candidates, all jets within $|\eta| < 4.5$ which are not also electron candidates, and all calorimeter clusters with $|\eta| < 4.5$ not associated to such objects.

Events are discarded if they contain any electrons or muons with $p_{\mathrm{T}} > 20$ GeV, or if they do not satisfy *cleaning cuts* designed to reject non-collision backgrounds [6]. In order to achieve maximal discovery reach for a wide variety of supersymmetric topologies, five signal regions are defined. Four signal regions characterised by increasing jet multiplicity requirements are defined as shown in Table 1, with the thresholds for the jets being $p_{\mathrm{T}} > 130$ GeV for the leading jet, corresponding to the trigger plateau, $p_{\mathrm{T}} > 40$ GeV for the remaining jets. The effective mass, $m_{\mathrm{eff}}$, is calculated as the sum of $E_{\mathrm{T}}^{\mathrm{miss}}$ and the magnitudes of the transverse momenta of the two, three or four highest $p_{\mathrm{T}}$ jets used to define the signal region. Two four-jet signal regions are defined requiring $m_{\mathrm{eff}} > 500$ GeV (optimised for small mass differences between SUSY mass states) and $m_{\mathrm{eff}} > 1000$ GeV (optimised for higher mass differences). In addition, a fifth 'high mass' signal region is derived from the four-jet sample, with more stringent requirements on the $p_{\mathrm{T}}$ of the non-leading jets ($> 80$ GeV) and on $m_{\mathrm{eff}}$ ($> 1100$ GeV), in order to give maximal reach in the SUSY mass spectrum. For this latter signal region the transverse momenta of all jets with $p_{\mathrm{T}} > 40$ GeV are used to compute $m_{\mathrm{eff}}$ (however, the $E_{\mathrm{T}}^{\mathrm{miss}}/m_{\mathrm{eff}}$ cut still uses only the leading four jets). In Table 1, $\Delta\phi(\mathrm{jet}, \vec{P}_{\mathrm{T}}^{\,\mathrm{miss}})_{\mathrm{min}}$ is the smallest of the azimuthal separations between $\vec{P}_{\mathrm{T}}^{\,\mathrm{miss}}$ and jets with $p_{\mathrm{T}} > 40$ GeV (all reconstructed jets up to a maximum of three, in descending order of $p_{\mathrm{T}}$).

| Signal Region | ≥ 2-jet 'A' | ≥ 3-jet 'B' | ≥ 4-jet 'C' / 'D' | High mass 'E' |
|---|---|---|---|---|
| $E_{\mathrm{T}}^{\mathrm{miss}}$ | > 130 | > 130 | > 130 | > 130 |
| Leading jet $p_{\mathrm{T}}$ | > 130 | > 130 | > 130 | > 130 |
| Second jet $p_{\mathrm{T}}$ | > 40 | > 40 | > 40 | > 80 |
| Third jet $p_{\mathrm{T}}$ | – | > 40 | > 40 | > 80 |
| Fourth jet $p_{\mathrm{T}}$ | – | – | > 40 | > 80 |
| $\Delta\phi(\mathrm{jet}, \vec{P}_{\mathrm{T}}^{\mathrm{miss}})_{\mathrm{min}}$ | > 0.4 | > 0.4 | > 0.4 | > 0.4 |
| $E_{\mathrm{T}}^{\mathrm{miss}}/m_{\mathrm{eff}}$ (leading 2, 3, 4 jets) | > 0.3 | > 0.25 | > 0.25 | > 0.2 |
| $m_{\mathrm{eff}}$ (leading 2, 3, 4 jets) | > 1000 | > 1000 | > 500/1000 | – |
| $m_{\mathrm{eff}}$ (jets with $p_{\mathrm{T}} > 40$ GeV) | – | – | – | > 1100 |
| Background events | 62.4 ± 10 | 54.9 ± 8.1 | 1015 ± 150/33.9 ± 6.8 | 13.1 ± 3.1 |
| Observed events | 58 | 59 | 1118/40 | 18 |
| Limit on $(\sigma \times A \times \varepsilon)$ / fb | 22 | 25 | 429/27 | 17 |

Table 1: Top rows: criteria for admission to each of the five overlapping signal regions ($m_{\mathrm{eff}}$, $E_{\mathrm{T}}^{\mathrm{miss}}$ and $p_{\mathrm{T}}$ in GeV). Bottom rows: expected background and observed event count, and extracted cross section upper limit for new physics at 95% C.L. ($A$ = acceptance, $\varepsilon$ = efficiency).

Standard Model background processes contribute to the event counts in the signal regions. The dominant sources are: $W$+jets, $Z$+jets, top quark pair ($t\bar{t}$), single top, and multi-jet production. In order to estimate the backgrounds in a consistent fashion, five control regions (CRs) are defined for each of the five signal regions (SRs), giving 25 CRs in total. Each ensemble of one SR and five CRs constitutes a different 'channel' of the analysis. For each channel, measurements in the CRs are used to derive background expectations in the SR through the use of 'transfer factors' equivalent to the ratios of expected event counts in the CRs and SR, derived independently of the data observations in the CR and SR. A combined likelihood fit across all control regions ensures that the background estimates are consistent for all processes, taking into account contamination of the CRs by multiple SM processes. The transfer factors are obtained from a combination of data and MC inputs.

The results of the analysis, i.e. the number of expected SM events and the number of observed events in each of the five signal regions, are given in Table 2 of Ref. [1], and summarised in the bottom rows of Table 1 here. The data are found to be in good agreement with the background expectation and no excess is observed. Therefore, limits on contributions of new physics to the signal regions are set. The bottom row of Table 1 shows upper limits on the effective cross section (production cross section $\sigma \times$ acceptance $A \times$ efficiency $\varepsilon$), assuming no signal uncertainties or contamination of the control regions.

The systematic uncertainties of the analysis are described in Ref. [1]. Dominant uncertainties on the background estimates include theoretical uncertainties on $W$+jets, $Z$+jets and $t\bar{t}$ production, the Jet Energy Scale/Resolution (JES/JER) and MC statistical uncertainties. Uncertainties on the signal acceptance include JES/JER variations, MC statistics, pileup reweighting and the application of the event cleaning cuts. Theoretical uncertainties on the signal cross section from varying the PDFs, $\alpha_S$ and the factorisation/renormalisation scale are also accounted for.

In the additional models described in this note, the mass-splittings between supersymmetric parents and decay products (particularly the LSP) are frequently small, limiting the amount of energy transferred to the visible decay products. With the hard kinematic cuts applied in the analysis, the modelling of

additional jet production from initial state radiation (ISR) can become an important factor driving the acceptance of signal events.

For this note, further studies have been done concerning the effects of ISR modelling on the signal acceptance and associated uncertainties. In these studies, $\tilde{g}\tilde{g}$ + jet and $\tilde{q}\tilde{q}$ + jet events have been generated with a matrix element approach as implemented in MadGraph 5 [7], matched to PYTHIA 6.4 [8] for parton showering, fragmentation and hadronization. A second set of events is generated without an extra jet in the matrix element, such that all additional jet radiation derives from the parton shower.

A comparison of these two samples shows no substantial differences in kinematic variables relevant to this analysis, such as jet $p_{\mathrm{T}}$ and $E_{\mathrm{T}}^{\mathrm{miss}}$, and hence no impacts on the signal acceptance beyond the 10% level, except for small squark and gluino masses ($M < 300$ GeV) and for small mass differences between the squark/gluino and the LSP ($\Delta M < 300$ GeV). In those cases, the parton shower approach underestimates the magnitude of the ISR and thus underestimates the acceptance of the analysis. The differences increase with decreasing squark/gluino mass and with decreasing mass gap between squark/gluino and LSP, and can ultimately be as large as $O(100\%)$ for signal selections that contribute to the final limit, particularly the 2-jet and 3-jet selections. The results presented in this note are derived using HERWIG++ for the calculation of the acceptance. The HERWIG++ approach, with which ATLAS produced large samples covering complete SUSY mass grids, is indistinguishable from PYTHIA. The results are thus conservative compared to the full matrix element approach.

While the acceptances based on HERWIG++ samples are conservative compared to those based on MadGraph/PYTHIA samples, our confidence in the acceptances is still based on the ISR modelling details in the latter matrix element approach. We therefore study the systematic uncertainties due to ISR by varying $\alpha_S$ and the MadGraph/PYTHIA matching parameters. The uncertainties are negligible at high masses and high mass splittings ($M > 300$ GeV and $\Delta M > 300$ GeV), and rise linearly with decreasing $M$ and decreasing $\Delta M$, to $\sim 30\%$ at $\Delta M = 0$ and $M > 300$ GeV, and $\sim 40\%$ at $M = 250$ GeV and $\Delta M = 0$. They are treated as uncorrelated with similar uncertainties on the background components, which gives more conservative results.

# 3 Interpretation in supersymmetric simplified models

Simplified models [9] are characterised by well-defined SUSY particle production and decay modes, and a minimal particle content for the final state under study. This can be achieved by assuming that all SUSY particles not of interest to a specific model are very massive and decouple. Multijet final states with missing transverse momentum but no leptons can be described by a number of simplified models. In this note, results are presented for the most basic ones. In the following models, the lightest neutralino $\tilde{\chi}_1^0$ is always the lightest supersymmetric particle (LSP), and R-parity conservation is assumed.

## 3.1 Model definition/Event generation

The simplified models by construction reduce the supersymmetric parameter space to a maximum of three free parameters, from the list below:

1. The mass of the degenerate first- and second-generation squarks, $m_{\tilde{q}}$.
2. The mass of the gluino, $m_{\tilde{g}}$.
3. The mass of the neutralino LSP, $m_{\tilde{\chi}_1^0}$.
4. The parameter $x$, defined as

$$x = \frac{m_{\tilde{\chi}_1^\pm} - m_{\tilde{\chi}_1^0}}{m_{\tilde{q}_L,\tilde{g}} - m_{\tilde{\chi}_1^0}}, \tag{1}$$

which controls the mass of the lighter chargino relative to the squark or gluino and the LSP.

Interpretation of the results in Ref. [1] is carried out in the following simplified models:

1. Pair production of first- and second-generation squarks decaying directly to quarks and the LSP ($\tilde{q}_{L,R} \to q\tilde{\chi}_1^0$) with 100% branching ratio. Squark masses 137.5 GeV $\leq m_{\tilde{q}} \leq$ 1200 GeV and LSP masses $0 \leq m_{\tilde{\chi}_1^0} \leq (m_{\tilde{q}} - 25$ GeV) are considered. The masses of all other particles, including gluinos and third-generation squarks, are set to 4.5 TeV.

2. Pair production of gluinos decaying directly to a quark-antiquark pair and the LSP ($\tilde{g} \to q\bar{q}\tilde{\chi}_1^0$), with 100% branching ratio. Gluino masses 137.5 GeV $\leq m_{\tilde{g}} \leq$ 1200 GeV and LSP masses $0 \leq m_{\tilde{\chi}_1^0} \leq (m_{\tilde{g}} - 25$ GeV) are considered. The masses of all other particles, including all squarks, are set to 4.5 TeV.

3. Production of first- and second-generation squarks decaying to a quark and a chargino, and subsequent decay of the chargino to an on- or off-shell W and the LSP ($\tilde{q}_L \to q\tilde{\chi}_1^\pm \to qW^{(*)}\tilde{\chi}_1^0$) with 100% branching ratio. Only left-handed squarks are considered, the couplings of the right-handed squarks to the chargino being forbidden. Squark masses 137.5 GeV $\leq m_{\tilde{q}} \leq$ 1200 GeV and LSP masses $0 \leq m_{\tilde{\chi}_1^0} \leq (m_{\tilde{q}} - 25$ GeV) are considered. Chargino masses are fixed by the values of $x = 1/4, 1/2, 3/4$, as defined in Eq. 1. The masses of other particles are set to 4.5 TeV.

4. Production of gluinos and analogous decays to a quark-antiquark pair and a chargino, and subsequent decay of the chargino to an on- or off-shell W and the LSP ($\tilde{g} \to q\bar{q}\tilde{\chi}_1^\pm \to q\bar{q}W^{(*)}\tilde{\chi}_1^0$) with 100% branching ratio. Gluino masses in the range 137.5 GeV $\leq m_{\tilde{g}} \leq$ 1200 GeV and LSP masses $0 \leq m_{\tilde{\chi}_1^0} \leq (m_{\tilde{g}} - 25$ GeV) are allowed. Chargino masses are fixed by the values of $x = 1/4, 1/2, 3/4$, as defined in Eq. 1. The masses of other particles are set to 4.5 TeV.

5. Production of first- and second-generation squarks and gluinos with direct two-body ($\tilde{q}_{L,R} \to q\tilde{\chi}_1^0$) or three-body decays ($\tilde{g} \to q\bar{q}\tilde{\chi}_1^0$), as in models 1 and 2. When kinematically allowed, the heavier strong sparticles may decay via the lighter ones, e.g. ($\tilde{q}_{L,R} \to q\,\tilde{g} \to q\bar{q}\tilde{\chi}_1^0$), ($\tilde{g} \to q\,\bar{\tilde{q}} \to \bar{q}\tilde{\chi}_1^0$). Planes in the squark and gluino masses with $m_{\tilde{\chi}_1^0} = 0, 195, 395$ GeV are probed with ($m_{\tilde{\chi}_1^0}$ + 5 GeV) $\leq m_{\tilde{q},\tilde{g}} \leq$ 2 TeV. All other particles have masses set to 5 TeV. The massless LSP case was presented in the results of the main analysis [1]. The processes of gluino-pair production, gluino-(anti)squark production, and squark-(anti)squark production are considered.

The choice of 137.5 GeV as a lower bound on the gluino or squark masses simulated is partly motivated by the bound of 100 GeV on $m_{\tilde{q}}$ from LEP. In addition, as the trigger selection implies cuts on the leading jet $p_{\mathrm{T}}$ and $E_{\mathrm{T}}^{\mathrm{miss}}$ of 130 GeV, the efficiency becomes vanishingly small for models in which the sparticle masses are lower. Precise values are set by the grid spacing.

Limits were previously placed on the one-step cascade models 3 and 4 by the ATLAS 2011 1-lepton analysis [10], which selected events where the decay of one of the W's in the cascade produced a lepton. In this analysis we consider the complementary event sample in which neither W decay was leptonic.

Events are generated with the `HERWIG++` v2.4.2 [11] Monte Carlo generator, based on SUSY Les Houches Accord (SLHA) files generated with `SUSYHIT` [12] (models 1,2,3,4) or `ISAJET`/`ISASUSY` [13] (model 5). Cross sections are determined with `PROSPINO` [14] at Next-to-Leading Order (NLO).

### 3.2 Results

The analysis of Ref. [1], summarised in Section 2, is used to constrain gluino and squark production in the simplified models. The combined likelihood fits to the data are repeated for all signal and control regions, taking into account for each model point the possible contamination of the control regions by

the SUSY signal. Plots of the experimental acceptance times efficiency ($A \times \varepsilon$) for the squark and gluino direct and one-step cascade decay grids can be found in Appendix A.

At each parameter point, we determine an upper limit on the production cross section times branching ratio ($\sigma \times BR$) for SUSY production. The computation takes into account all background uncertainties as well as experimental uncertainties on the signal expectation. Theoretical uncertainties on the production cross section are ignored for this upper limit. However, they are incorporated into the computation of limit contours, which assume the nominal MSSM cross sections for the specific models. Results for different signal regions are combined by selecting the signal region with the best expected cross section limit at each parameter point.

Results for models 1, 2, 3 and 4 are shown in Figures 1 and 2. Figures 3 and 4 illustrate the signal selections having the best sensitivity, and hence contributing to the bounds, at each model point. Additional limit plots for each of the individual signal selections are shown in Appendix B. The results for model 5 are shown in Figure 5, with the optimal signal selections shown in Figure 6.

### 3.3 Discussion

Interpretation of the 2011 ATLAS 0-lepton [1] analysis in terms of simplified models reveals strengths and limitations of the search when dealing with multiple production modes and decay topologies.

Better cross section limits are achieved on direct decay modes of squarks and gluinos than on the one-step decay modes. For both squarks and gluinos, the selection is effective for LSP masses up to approximately 200 GeV (slightly higher for the gluino models, slightly lower for the squark models), but for higher LSP masses the squark and gluino limits soften or are absent.

At the 95% Confidence Level (C.L), gluino (squark) masses below 700 (650) GeV are excluded for LSP masses up to 200 GeV assuming direct decays, with the squark (gluino) mass set to 4.5 TeV. When the gluino decays via an intermediate chargino of moderate mass (with the parameter $x = 1/2, 3/4$), the gluino mass is constrained to be above $600 - 700$ GeV for LSP masses up to 100 GeV.

For the one-step decay modes, and in particular for $x = 1/4$, i.e. small mass differences between chargino and LSP, the interesting feature appears that the acceptance is better for non-zero LSP masses than for a massless LSP. This is due to the rate at which the compression affects the spectrum of the $E_{\mathrm{T}}^{\mathrm{miss}}$ versus that of the $m_{\mathrm{eff}}$, and the consequences on the efficiency of the cut on $E_{\mathrm{T}}^{\mathrm{miss}}/m_{\mathrm{eff}}$ [17]. This is illustrated in Figures 11 and 14, where the acceptance increases from $m_{\mathrm{LSP}} = 0$ to values of 200-400 GeV, depending on the signal selection, before falling away as the spectrum becomes increasingly degenerate.

For the one-step squark decays, the obtained cross section limits are higher than the nominal production cross section, and no exclusion can be made. Both squark results are, however, sensitive to assumptions about the gluino mass, as the important $t$-channel gluino exchange diagram becomes suppressed for heavy gluinos, reducing the squark production cross section.

When both squark and gluino production are allowed, the degradation of the limits due to higher LSP masses is more limited, particularly when the squark and gluino masses are similar enough that the associated production process dominates the SUSY production. This is primarily because above mass-splittings of $\sim 600$ GeV, the selection efficiency is relatively constant with respect to the mass scale, and hence the production cross section (which is flat for varying degrees of compression) largely determines the maximal reach of the analysis. Equal-mass squarks and gluinos lighter than 1025 GeV are excluded.

Surprisingly, the analysis is able to exclude models with spectra in which the lighter superpartner has as small a mass-splitting with the LSP as 5 GeV, e.g. 400 GeV squarks or gluinos, with $m_{\mathrm{LSP}} = 395$ GeV. Such models are not excluded in the case of exclusive squark or gluino production. In the case that both sparticles are very light, e.g. $m_{\tilde{q}} = m_{\tilde{g}} = 400$ GeV, the sensitivity is virtually all due to ISR. From figures 1 and 2, it can be seen that approximately a 30 pb cross section is needed for exclusion. In the absence of associated production, the squark and gluino cross sections sum to 21 pb, and hence even together

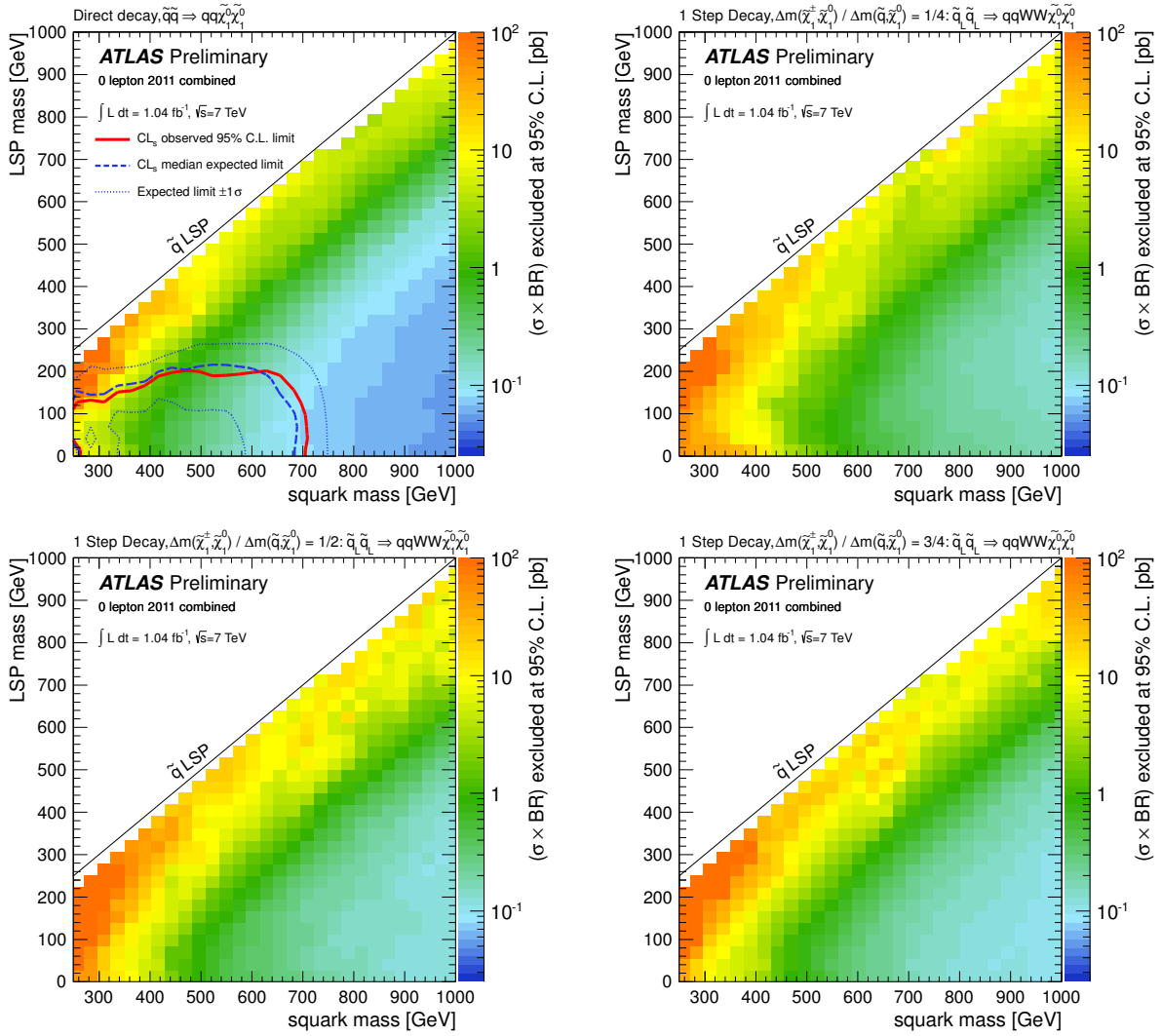


Figure 1: Exclusion limits in the $\tilde{q} - \tilde{\chi}_1^0$ mass plane for direct [top left] and one-step squark decays with the chargino mass parameter $x = 1/4, 1/2$ and $3/4$ [top right, bottom left and bottom right respectively]. The colour scale shows the combined limit on the cross section times branching ratio ($\sigma \times BR$) at the 95% C.L from all five signal regions, determined using the result from the signal region providing the best *expected* limit for each point. The expected and observed limits assuming the NLO cross section from supersymmetric QCD and 100% branching fraction are shown as blue and red contours respectively. In the case of direct decays, the cross section for $\tilde{q}_{L,R}$ production is assumed, however, $\tilde{q}_R$ production is neglected for the one-step cascade grids, effectively halving the production cross section. This only applies to the limit contours. For the one-step cascade grids, the nominal cross sections are too low for any model points to be excluded at 95% C.L., hence no limit contours are drawn.

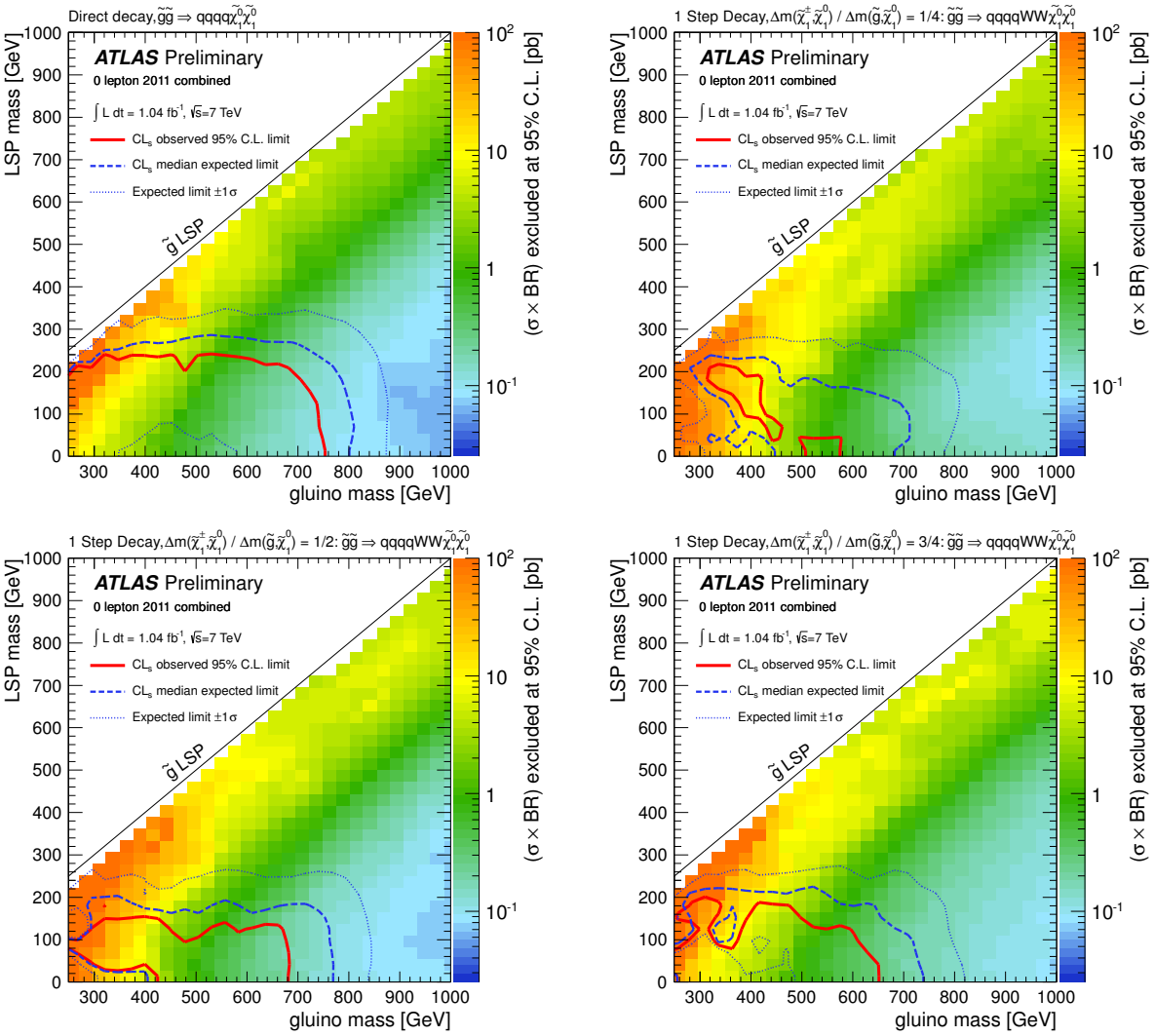


Figure 2: Exclusion limits in the $\tilde{g} - \tilde{\chi}_1^0$ mass plane for direct [top left] and one-step gluino decays with the chargino mass parameter $x = 1/4, 1/2$ and $3/4$ [top right, bottom left and bottom right respectively]. The colour scale shows the combined limit on the cross section times branching ratio ($\sigma \times BR$) at the 95% C.L from all five signal regions, determined using the result from the signal region providing the best *expected* limit for each point. The expected and observed limits assuming the NLO cross section from supersymmetric QCD and 100% branching fraction are shown as blue and red contours respectively.

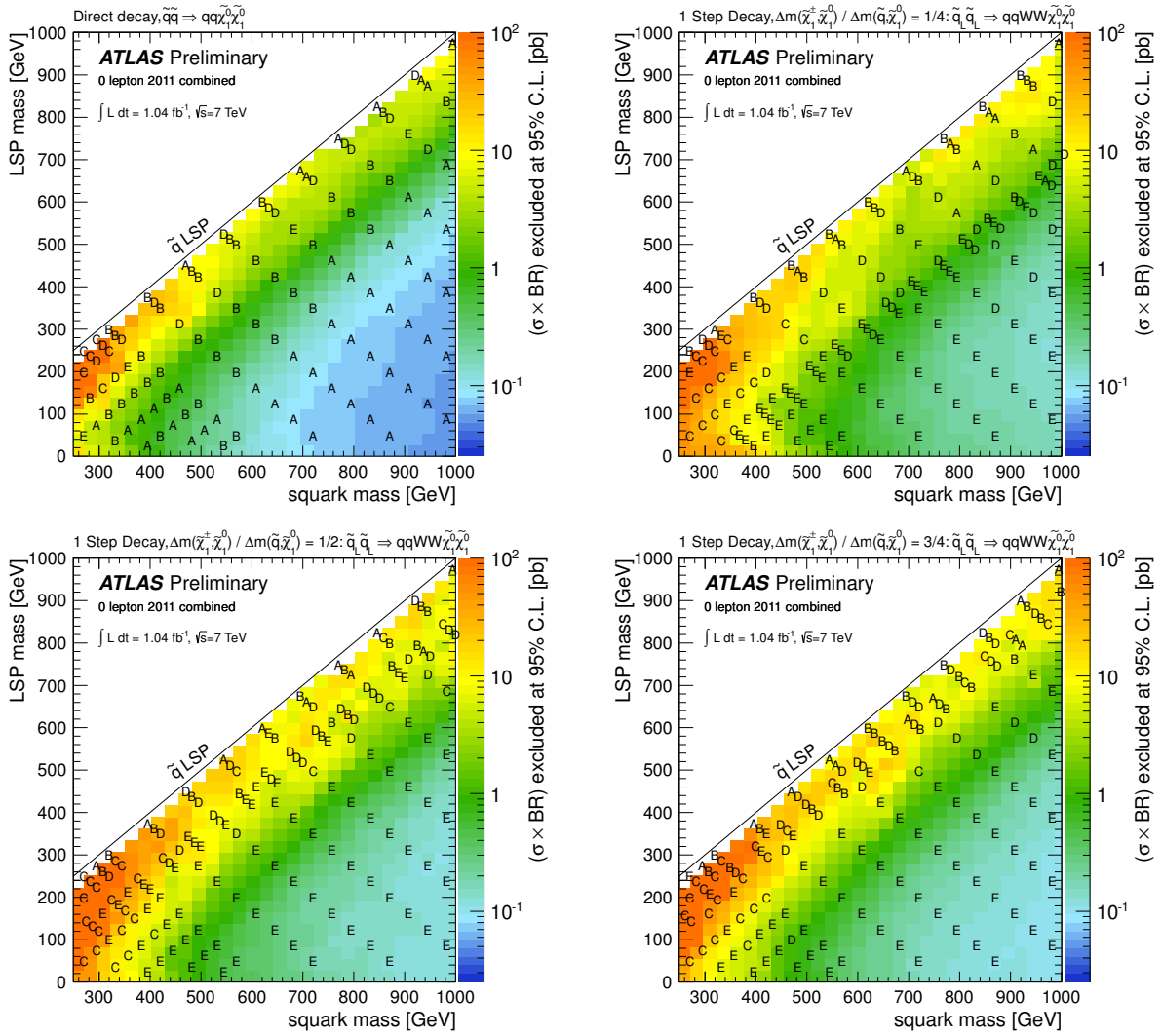


Figure 3: Signal regions providing the best *expected* limit in the $\tilde{q} - \tilde{\chi}_1^0$ mass plane for direct [top left] and one-step squark decays with the chargino mass parameter $x = 1/4, 1/2$ and $3/4$ [top right, bottom left and bottom right respectively]. Signal regions are indicated by the symbols: A – 2-jet selection, B – 3-jet selection, C – 4-jet soft selection, D – 4-jet hard selection, E – high-mass selection, as defined in Table 1. The colour scale shows the combined limit on the cross section times branching ratio ($\sigma \times BR$), corresponding to the limit from the indicated SR.

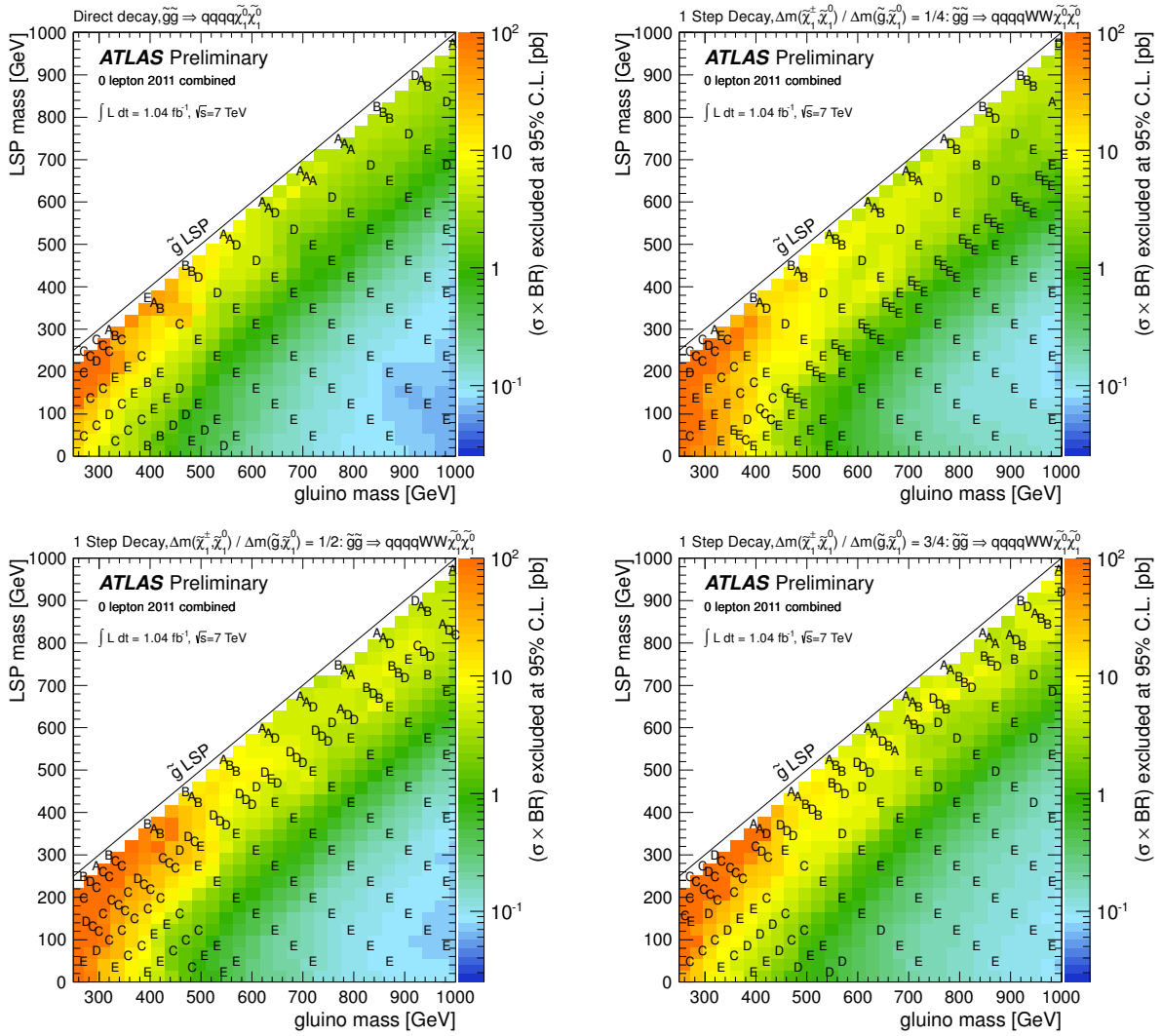


Figure 4: Signal regions providing the best *expected* limit in the $\tilde{g} - \tilde{\chi}_1^0$ mass plane for direct [top left] and one-step gluino decays with the chargino mass parameter $x = 1/4, 1/2$ and $3/4$ [top right, bottom left and bottom right respectively]. Signal regions are indicated by the symbols: A – 2-jet selection, B – 3-jet selection, C – 4-jet soft selection, D – 4-jet hard selection, E – high-mass selection, as defined in Table 1. The colour scale shows the combined limit on the cross section times branching ratio ($\sigma \times BR$), corresponding to the limit from the indicated SR.

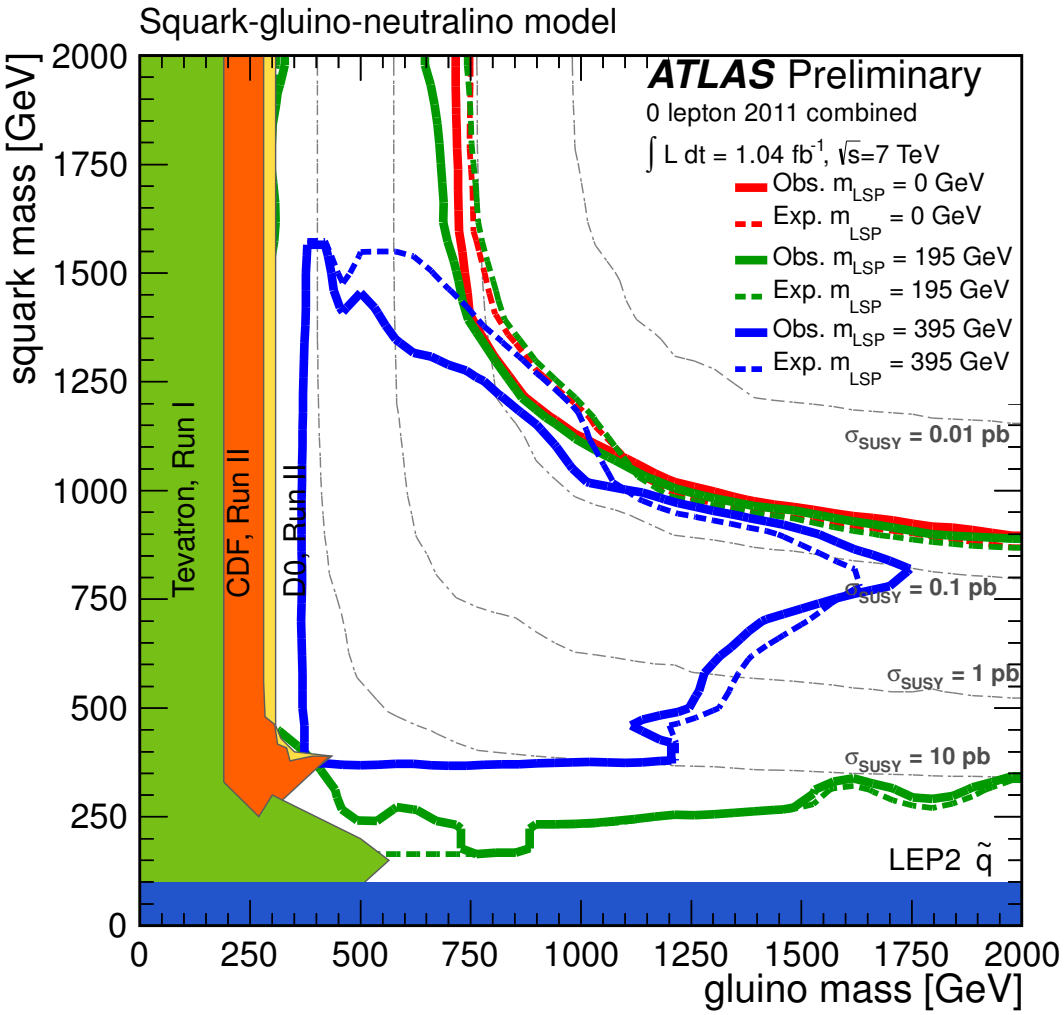


Figure 5: Combined exclusion limits in the $\tilde{q}-\tilde{g}$ mass plane for various values of the $\tilde{\chi}_1^0$ LSP mass. Three hypotheses for the neutralino LSP mass are shown, in red, green and blue for $m_{\mathrm{LSP}} = 0$, 195 and 395 GeV respectively. Observed limits are shown by solid lines, whereas expected limits are dashed. The lines of no exclusion at low squark or gluino masses in the $m_{\mathrm{LSP}} > 0$ cases appear because models with $m_{\tilde{g}}, m_{\tilde{q}}$ below the $\tilde{\chi}_1^0$ mass are not generated. Existing constraints from the Tevatron [15] and LEP [16] experiments are also shown. However, the Tevatron limits were derived in the context of CMSSM/MSUGRA models with a fixed mass ratio between the gluino/squark and neutralino, and are not directly comparable with the models defined by ATLAS.

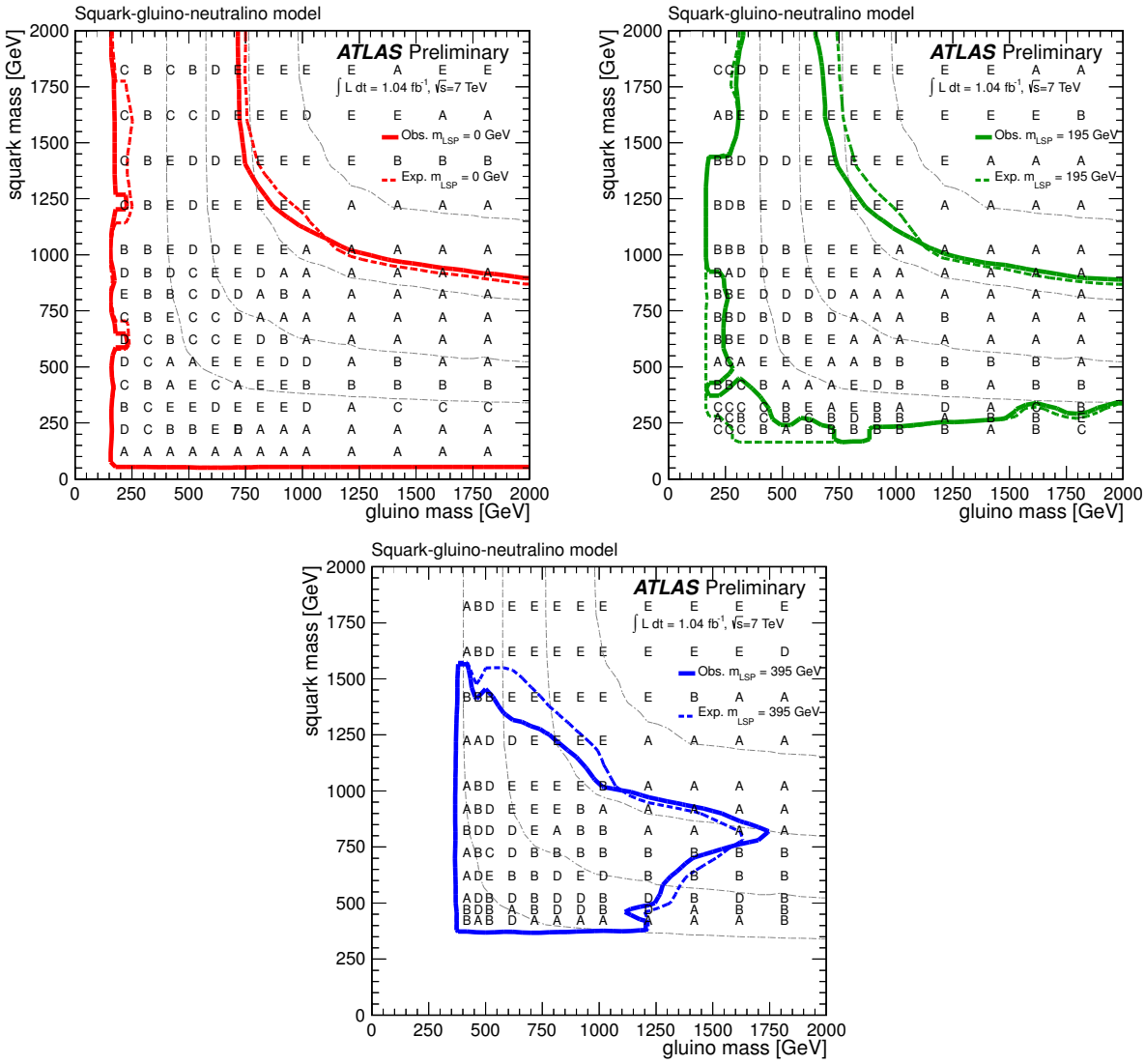


Figure 6: Signal regions providing the best *expected* limit in the $\tilde{q} - \tilde{g}$ mass plane for various values of the $\tilde{\chi}_1^0$ LSP mass. Three hypotheses for the neutralino LSP mass are shown, in red, green and blue for $m_{\text{LSP}} = 0, 195$ and 395 GeV respectively. Observed limits are shown by solid lines, whereas expected limits are dashed.

they cannot be excluded. However, associated $\tilde{q}\tilde{g}$ production provides another 25 pb of cross section, allowing the point to be excluded.

Furthermore, even when one superpartner is considerably heavier, the analysis retains sensitivity to associated production. For example, the threshold for production of 1400 GeV squarks with 400 GeV gluinos is comparable to that for pair-producing 900 GeV gluinos or squarks, and the mass-splitting of the heavier sparticle is large enough to give a high efficiency, even when the LSP is quite degenerate with the lighter sparticle. Hence points such as ($m_{\tilde{q}} = 1400$ GeV, $m_{\tilde{g}} = 400$ GeV, $m_{\mathrm{LSP}} = 395$ GeV) can be excluded in spite of the high compression of the gluinos.

More interesting phenomenology is apparent in the 395 GeV LSP grid. Without associated production, one would expect the limits for small $m_{\tilde{g},\tilde{q}}$ to become constant for large $m_{\tilde{q},\tilde{g}}$, once the heavier sparticle decouples. Instead, the exclusion on large $m_{\tilde{q}}$ ($\sim 1.3 - 1.5$ TeV) is maximal for light gluinos, and degrades towards the equal-mass limit, whereas it increases in large $m_{\tilde{g}}$ ($\sim 1.2 - 1.7$ TeV) as $m_{\tilde{q}}$ rises, up to a maximum at $m_{\tilde{q}} = 800$ GeV. The falling overall cross section is partly responsible for the large $m_{\tilde{q}}$ behaviour. At low gluino masses, the associated production bolsters the efficiency until the mass-splitting becomes large enough that the intrinsic efficiency for gluino pair-production takes over. The cross section for associated production diminishes more swiftly for large gluino masses, and hence there is less of an increase in sensitivity when the squarks are degenerate with the LSP. Hence, in the large $m_{\tilde{g}}$ region, the efficiency of selecting $\tilde{q}\tilde{q}$ events is the dominant factor determining the search sensitivity.

# 4 Interpretation in Minimal Universal Extra Dimensions

In the Minimal Universal Extra Dimensions model [18, 19, 20] the Standard Model fields are allowed to propagate into $4 + \delta$ dimensions, the extra dimensions being compactified at a scale equivalent to the reciprocal of the size of the extra dimensions, $R^{-1}$. The model is fully determined by the values of $R^{-1}$ and a cutoff scale $\Lambda$. From a phenomenological point of view there are many parallels between the MUED and SUSY models. In the MUED model, each SM field has Kaluza-Klein (KK) partners that, in contrast to SUSY, have the same spin. In this analysis, only the first KK level is considered for each SM particle. For brevity, henceforth "KK particle" denotes the first KK partner.

Momentum conservation in the extra dimensions implies the conservation of a KK quantum number – the KK parity – so that KK particles are also always produced in pairs. Heavier KK-particles successively decay into the lightest KK particle (LKP) and SM particles. The LKP escapes detection, leading to missing transverse energy signatures. The masses of all MUED particles are, to lowest order, $m_{\mathrm{KK}} = \sqrt{m_{\mathrm{SM}}^2 + R^{-2}}$, where $m_{\mathrm{SM}}$ is the mass of the corresponding Standard Model particle. The theory is governed by a cutoff scale $\Lambda > R^{-1}$ above which it is no longer perturbative. The masses of the KK particles receive radiative corrections proportional to $\ln(\Lambda \cdot R)$ [19]. A typical spectrum and its dependence on $\Lambda \cdot R$ is shown in Ref. [20]. The LKP, denoted as the KK photon $\gamma_{\mathrm{KK}}$, receives only small corrections, whereas the KK gluon $g_{\mathrm{KK}}$ receives large corrections. For low values of $\Lambda \cdot R$, the spectrum is compressed, in analogy with compressed SUSY spectra.

## 4.1 Model definition/Event generation

In the framework of this analysis, the Minimal MUED scenario with one additional extra dimension ($\delta = 1$) is studied, as implemented in the HERWIG++ v2.4.2 Monte Carlo generator, which takes into account the particle spin correlations. All samples are generated at $\sqrt{s} = 7$ TeV and passed through the full ATLAS detector simulation and reconstruction. Only points with $300 \leq R^{-1} \leq 900$ GeV are considered, values below 300 GeV being excluded by electroweak fits to the Tevatron and LEP data [18]. The parameter $\Lambda \cdot R$ is varied between 2 and 40. For $\Lambda \cdot R \gtrsim 30$, the effective theory becomes non-perturbative [18]. Typically, $\Lambda \cdot R$ is restricted to a range between 10 and 20. We explore this larger range

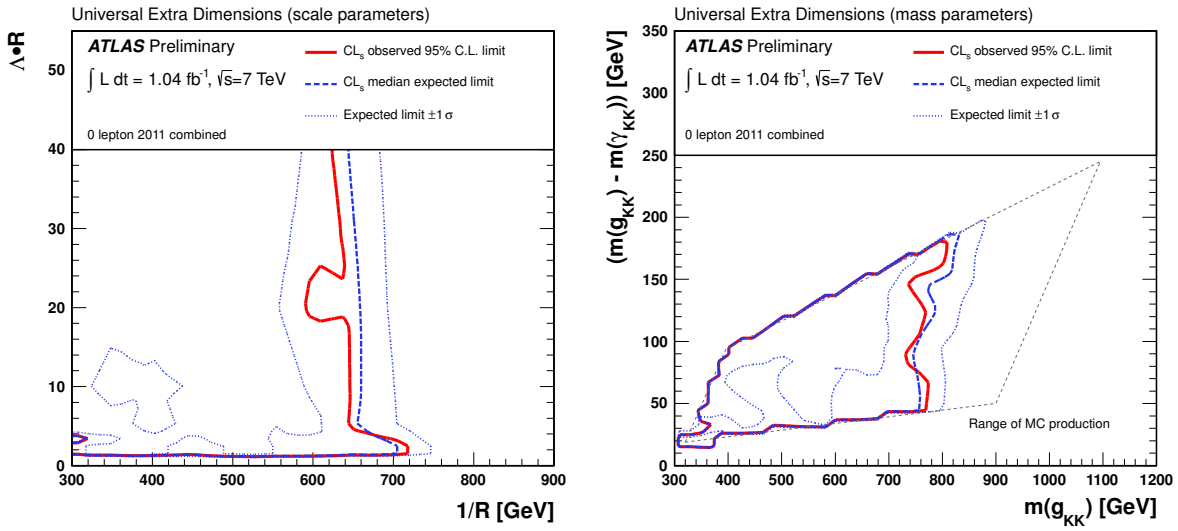


Figure 7: Exclusion limits in the Universal Extra Dimensions model space, in terms of [left] the compactification scale ($R^{-1}$) and the compression scale ($\Lambda \cdot R$) and [right] the masses of the Kaluza-Klein gluon $g_{\mathrm{KK}}$ and the Kaluza-Klein photon $\gamma_{\mathrm{KK}}$ (LKP). All cross sections are computed at leading order. In the mass parameter plot, the ranges of the MC simulation in the right hand plot are indicated in dashed lines. The lines correspond to the edges of the left-hand plot.

in order to test the dependence of our limits on the value of $\Lambda \cdot R$ independently of theoretical preferences. Currently there are no NLO calculations for the minimal MUED model available, therefore only LO HERWIG++ cross sections are used, and theoretical uncertainties are not applied. Only experimental uncertainties on the signal acceptance are considered.

As an alternative representation, the limits on the MUED scenarios are also shown versus mass parameters, namely the mass of the Kaluza-Klein gluon $m_{g_{KK}}$ and the mass-difference between the KK gluon and KK photon, $\Delta m(g_{KK}, \gamma_{KK})$. The same signal MC points are used, meaning that the regular grid in $R^{-1}$, $\Lambda \cdot R$ is mapped to an irregular quadrilateral in the mass parameters whose edges match the ranges on the fundamental parameters.

## 4.2 Results

The analysis of Ref. [1] is used to constrain Kaluza-Klein gluon production and decay in MUED in a way analogous to the method presented for the simplified models. The exclusion limits in terms of the compactification scale of the extra dimensions $R^{-1}$ and the compression scale $\Lambda \cdot R$, or alternatively the masses of $m_{g_{KK}}$ and $\Delta m(g_{KK}, \gamma_{KK})$ are shown in Figure 7. The signal selections contributing to the limits are illustrated in Figure 8.

## 4.3 Discussion

In a MUED model, a bound of 600 GeV is set on the compactification scale $R^{-1}$, for values of the compression scale $\Lambda \cdot R$ between 2 and 40, translating to a lower bound of 730 GeV on the mass of the Kaluza-Klein gluon. This bound is set for $\Lambda \cdot R \simeq 20$, which gives the most conservative estimate. It should be noted that the cross sections used for MUED models are computed only at leading order, and the results quoted in this note might be altered by next-to-leading order corrections.

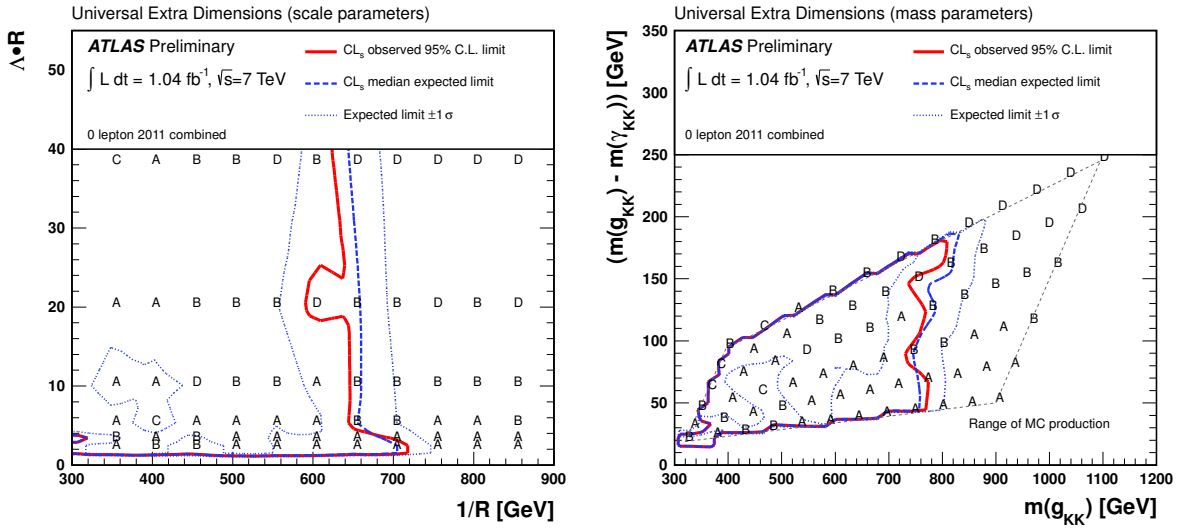


Figure 8: Signal regions providing the best *expected* limit in the Universal Extra Dimensions model space, in terms of [left] the compactification scale ($R^{-1}$) and the compression scale ($\Lambda \cdot R$) and [right] the masses of the Kaluza-Klein gluon $g_{\mathrm{KK}}$ and the Kaluza-Klein photon $\gamma_{\mathrm{KK}}$ (LKP). Signal regions are indicated by the symbols: A – 2-jet selection, B – 3-jet selection, C – 4-jet soft selection, D – 4-jet hard selection, E – high-mass selection, as defined in Table 1. The expected and observed limits assuming the LO cross section are shown as blue and red contours respectively. In the mass parameter plot, the ranges of the MC simulation in the right hand plot are indicated in dashed lines. The lines correspond to the edges of the left-hand plot.

The limits placed on MUED scenarios by this analysis are the most stringent from direct searches to date. Previous searches have placed limits on *non-minimal* Universal Extra Dimensions scenarios. The most recent are from ATLAS diphoton searches, in which a limit of 946 GeV is set on $R^{-1}$ [21]. It should be stressed, however, that the diphoton limit makes different assumptions from those made in the current note. Specifically, it is assumed that the single-UED model is embedded in a 6-dimensional space, opening up gravitational decays for the KK photon to a SM photon and gravitino. Such decays are forbidden in the MUED framework.

Compressed MUED models are found to be better constrained by the 0-lepton analysis relative to similarly compressed SUSY simplified models. However, the comparison should be made with some caution, as the models are not directly comparable. Firstly, the spin structure of the MUED particle spectrum yields an increase of roughly a factor of five for KK quark production relative to squarks of equivalent mass. Furthermore, the expanded particle spectrum relative to the SUSY simplified models provides for an increased total cross section.

# 5 Conclusion

The extension of the ATLAS 0-lepton analysis [1] to compressed spectra demonstrates substantial sensitivity to mass-degenerate models.

Lower bounds of 700 (650) GeV can be set on the masses of gluinos (squarks) decaying directly to quarks and an LSP of mass up to 200 GeV, where the squark (gluino) mass is set to 4.5 TeV. The gluino limit is softened to 600 GeV given an LSP mass of 100 GeV for one-step cascade decays via a moderately massive intermediate chargino. Gluino decays via light charginos and left-handed squark cascade decays yield poorer or nonexistent bounds at the nominal cross section.

The analysis is more sensitive to models with associated squark/gluino production, in which a limit of 1025 GeV can be placed on equal-mass squarks and gluinos.

A single universal extra dimension, with no additional gravitational interactions, is constrained to have compactification scale $R^{-1} > 600$ GeV for $2 \leq \Lambda \cdot R \leq 40$. This yields a lower limit of 730 GeV on the mass of the first KK gluon.

# References


[1] The ATLAS Collaboration, *Search for squarks and gluinos using final states with jets and missing transverse momentum with the ATLAS detector in* $\sqrt{s} = 7$ *TeV proton-proton collisions*, arXiv:1109.6572 (2011).

[2] W. Lampl, S. Laplace, D. Lelas, P. Loch, H. Ma, S. Menke, S. Rajagopalan, D. Rousseau, S. Snyder, and G. Unal, *Calorimeter Clustering Algorithms: Description and Performance*, ATL-LARG-PUB-2008-002.

[3] M. Cacciari, G. P. Salam and G. Soyez, *The anti-$k_t$ jet clustering algorithm*, JHEP **04** (2008) 063. M. Cacciari and G. P. Salam, *Dispelling the $N^3$ myth for the $k_t$ jet-finder*, Phys. Lett. **B641** (2006) 57.

[4] The ATLAS Collaboration, *Jet energy scale and its systematic uncertainty in proton-proton collisions at* $\sqrt{s} = 7$ *TeV in ATLAS 2010 data*, ATLAS-CONF-2011-032.

[5] The ATLAS Collaboration, *Measurement of the* $W \to l\nu$ *and* $Z/\gamma^* \to ll$ *production cross sections in proton-proton collisions at* $\sqrt{s} = 7$ TeV *with the ATLAS detector*, JHEP **12** (2010) 060.

[6] The ATLAS Collaboration, *Data-Quality Requirements and Event Cleaning for Jets and Missing Transverse Energy Reconstruction with the ATLAS Detector in Proton-Proton Collisions at a Center-of-Mass Energy of* $\sqrt{s} = 7$ *TeV*, ATLAS-CONF-2010-038.

[7] J. Alwall et al., *MadGraph 5: going beyond*, JHEP **06** (2011) 128.

[8] T. Sjostrand, S. Mrenna and P. Skands, *PYTHIA 6.4 physics and manual*, JHEP **05** (2006) 026.

[9] J. Alwall, P. Schuster and N. Toro, *Simplified models for a first characterization of new physics at the LHC*, Phys. Rev. D **79** (2009) 075020.
D. Alves et al., *Simplified Models for LHC New Physics Searches*, arXiv:1105.2838 [hep-ph] (2011).

[10] The ATLAS Collaboration, *Search for supersymmetry in final states with jets, missing transverse momentum and one isolated lepton in* $\sqrt{s} = 7$ *TeV pp collisions using 1* $fb^{-1}$ *of ATLAS data*, arXiv:1109.6606 (2011).

[11] M. Bahr et al., *Herwig++ Physics and Manual*, Eur. Phys. J. **C58** (2008) 639–707.
M. Bahr et al., *Herwig++ 2.3 release note, arXiv:0812.0529*, 0812.0529, 2008.

[12] A. Djouadi, M. M. Muhlleitner and M. Spira, *Decays of Supersymmetric Particles: the program SUSY-HIT (SUspect-SdecaY-Hdecay-InTerface)*, arXiv:hep-ph/0609292 (2006).

[13] F. E. Paige, S. D. Protopopescu, H. Baer, and X. Tata, *ISAJET 7.69: A Monte Carlo event generator for p p, anti-p p, and e+ e- reactions*, `arXiv:0312045 [hep-ph]`.

[14] W. Beenakker, R. Hopker, M. Spira and P. M. Zerwas, *Squark and gluino production at hadron colliders*, Nucl. Phys. B **492** (1997) 51.

[15] The CDF Collaboration, *Inclusive Search for Squark and Gluino Production in* $p\bar{p}$ *Collisions at* $\sqrt{s} = 1.96$*-TeV*, Phys. Rev. Lett. **102** (2009) 121801.
The D0 Collaboration, *Search for squarks and gluinos in events with jets and missing transverse energy using 2.1* $fb^{-1}$ *of* $p\bar{p}$ *collision data at* $\sqrt{s} = 1.96$ *TeV*, Phys. Lett. **B660** (2008) 449–457.
The D0 Collaboration, *Search for squarks and gluinos in* $p\bar{p}$ *collisions at* $\sqrt{s} = 1.8$ *TeV*, Phys. Rev. Lett. **75** (1995) 618–623.
The CDF Collaboration, *Search for gluinos and scalar quarks in* $p\bar{p}$ *collisions at* $\sqrt{s} = 1.8$ *TeV using the missing energy plus multijets signature*, Phys. Rev. Lett. **88** (2002) 041801.

[16] The DELPHI Collaboration, *Searches for supersymmetric particles in e+ e- collisions up to 208 GeV and interpretation of the results within the MSSM*, Eur.Phys.J. **C31** (2003) 421–479.
The L3 Collaboration, *Search for scalar leptons and scalar quarks at LEP*, Phys.Lett. **B580** (2004) 37–49.

[17] T. J. LeCompte and S. P. Martin, *Large Hadron Collider reach for supersymmetric models with compressed mass spectra*, Phys. Rev. **D84** (2011) 015004.

[18] T. Appelquist, H.-C. Cheng, and B. A. Dobrescu, *Bounds on universal extra dimensions*, Phys. Rev. **D64** (2001) 035002.

[19] D. Hooper and S. Profumo, *Dark Matter and Collider Phenomenology of Universal Extra Dimensions*, Phys. Rept. **453** (2007) 29.

[20] H.-C. Cheng, K. T. Matchev and M. Schmaltz, *Bosonic Supersymmetry? Getting Fooled at the LHC*, Phys. Rev. D **66** (2002) 056006.

[21] The ATLAS Collaboration, *Search for Diphoton Events with Large Missing Transverse Energy with* $36pb^{-1}$ *of 7 TeV Proton-Proton Collision Data with the ATLAS Detector*, Eur. Phys. J. **C71** (2011) 1744.

# A Acceptance times efficiency plots

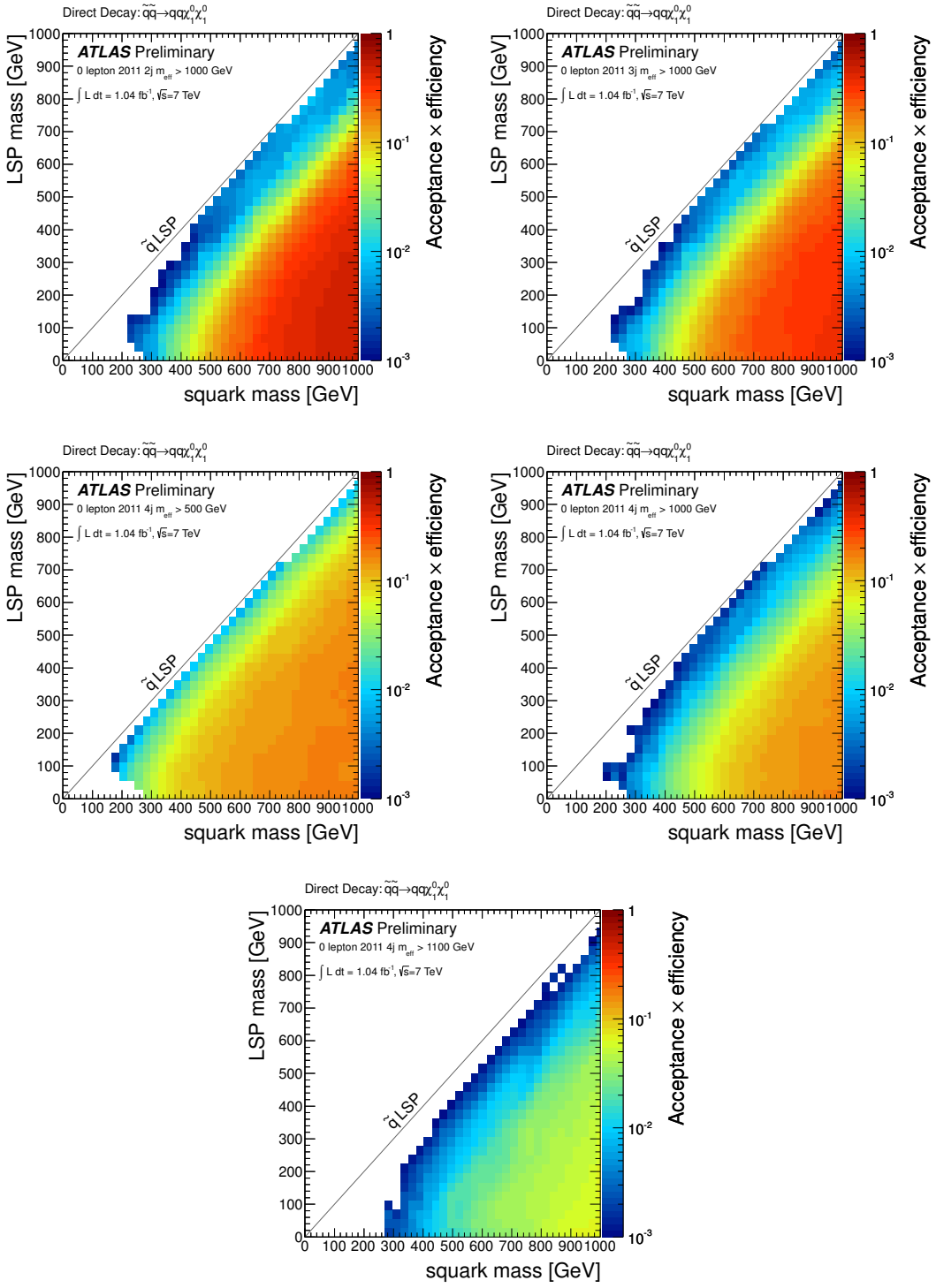


Figure 9: Acceptance times efficiency ($A \times \varepsilon$), defined as the fraction of signal events passing full event selection in the $\tilde{q} - \tilde{\chi}_1^0$ mass plane for direct squark decays $\tilde{q} \to q\tilde{\chi}_1^0$ for each of the five signal selections. Points shown in white have less than 0.1% of events accepted.

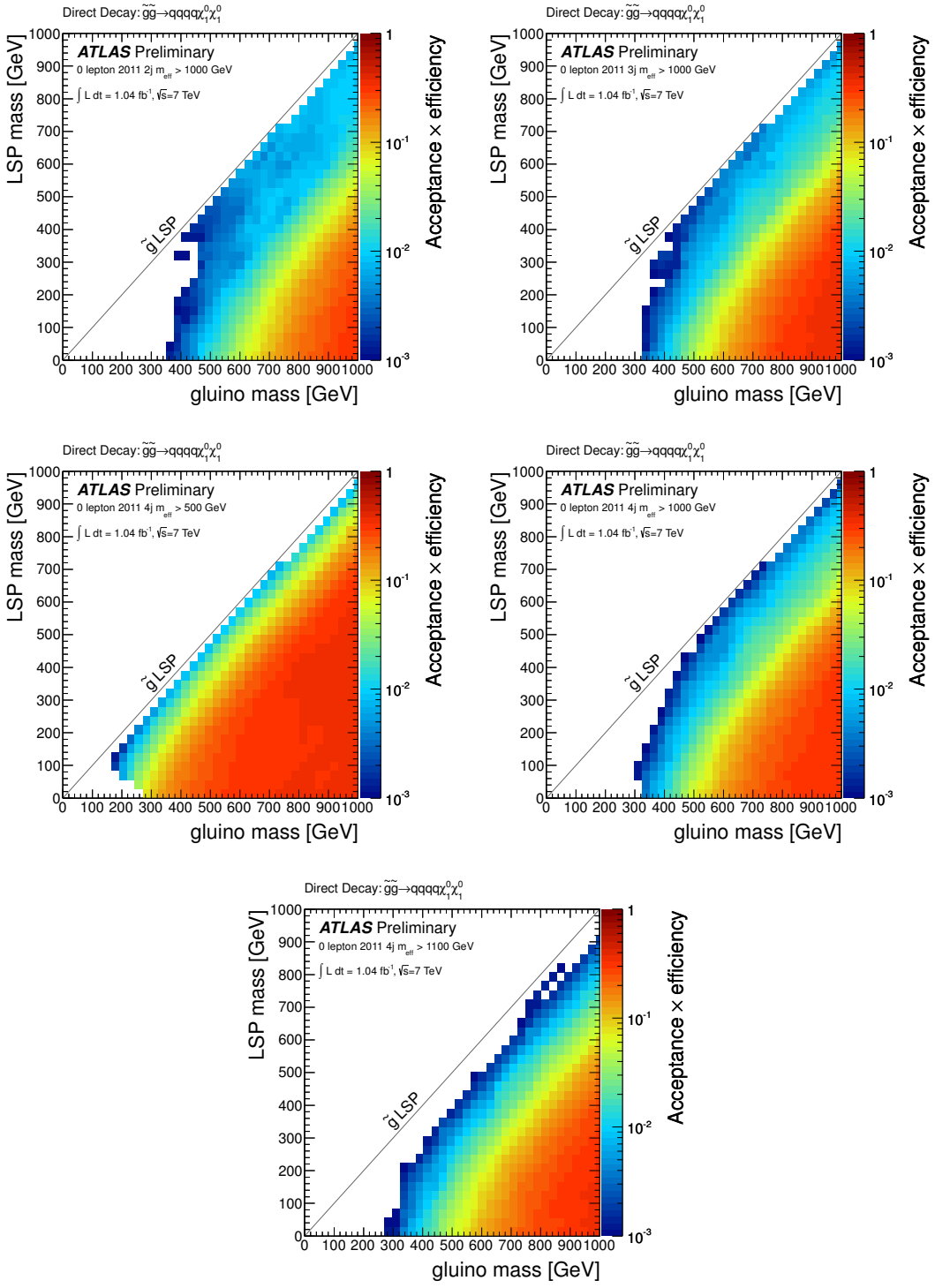


Figure 10: Acceptance times efficiency ($A \times \varepsilon$), defined as the fraction of signal events passing full event selection in the $\tilde{g}-\tilde{\chi}_1^0$ mass plane for direct gluino decays $\tilde{g} \to q\bar{q}\tilde{\chi}_1^0$ for each of the five signal selections. Points shown in white have less than 0.1% of events accepted.

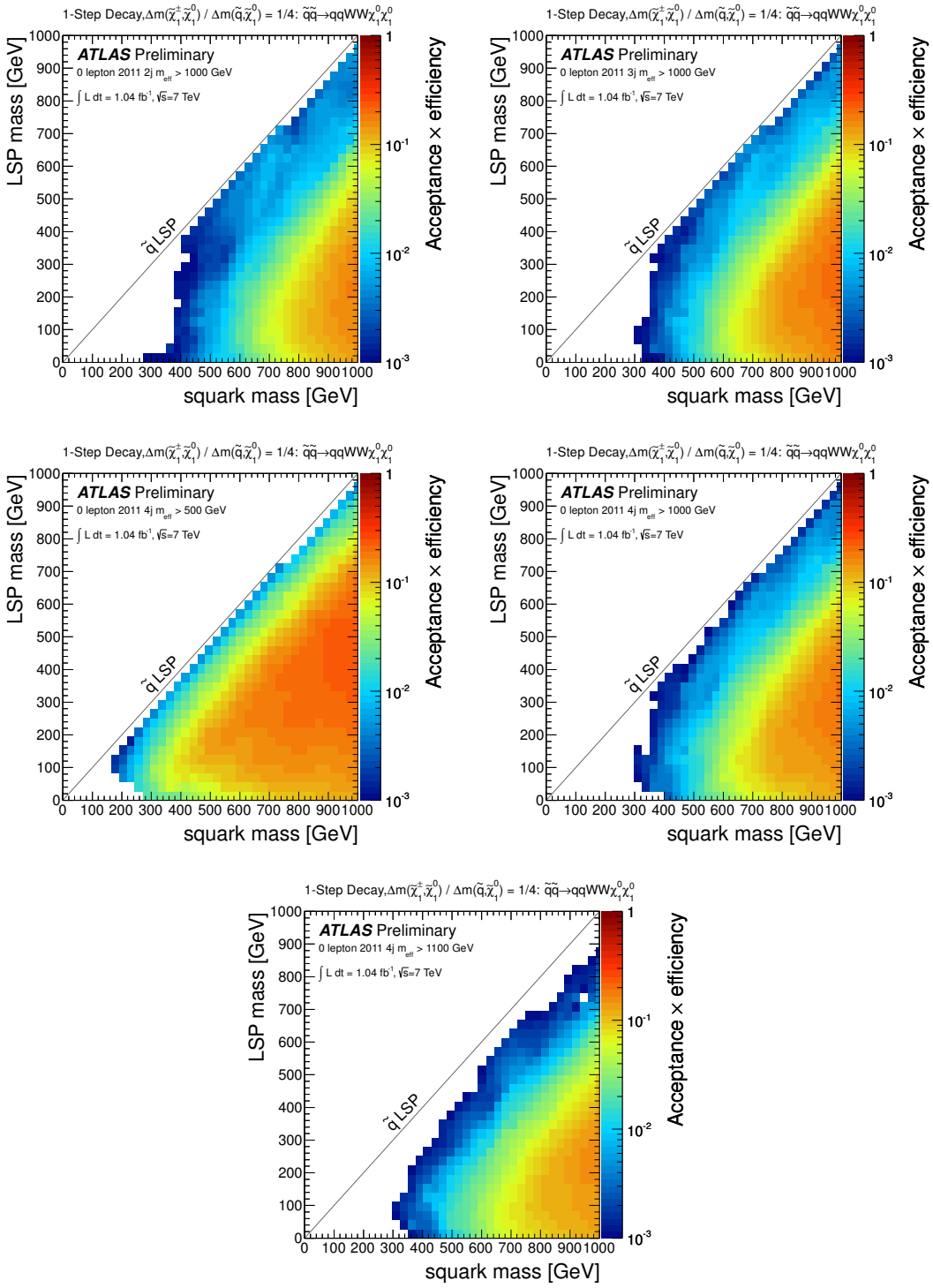


Figure 11: Acceptance times efficiency ($A \times \varepsilon$), defined as the fraction of signal events passing full event selection in the $\tilde{q} - \tilde{\chi}_1^0$ mass plane for one-step squark decays $\tilde{q} \to q\tilde{\chi}_1^{\pm} \to q\, W^{\pm} \tilde{\chi}_1^0$ with $x = 1/4$ for each of the five signal selections. Points shown in white have less than 0.1% of events accepted.

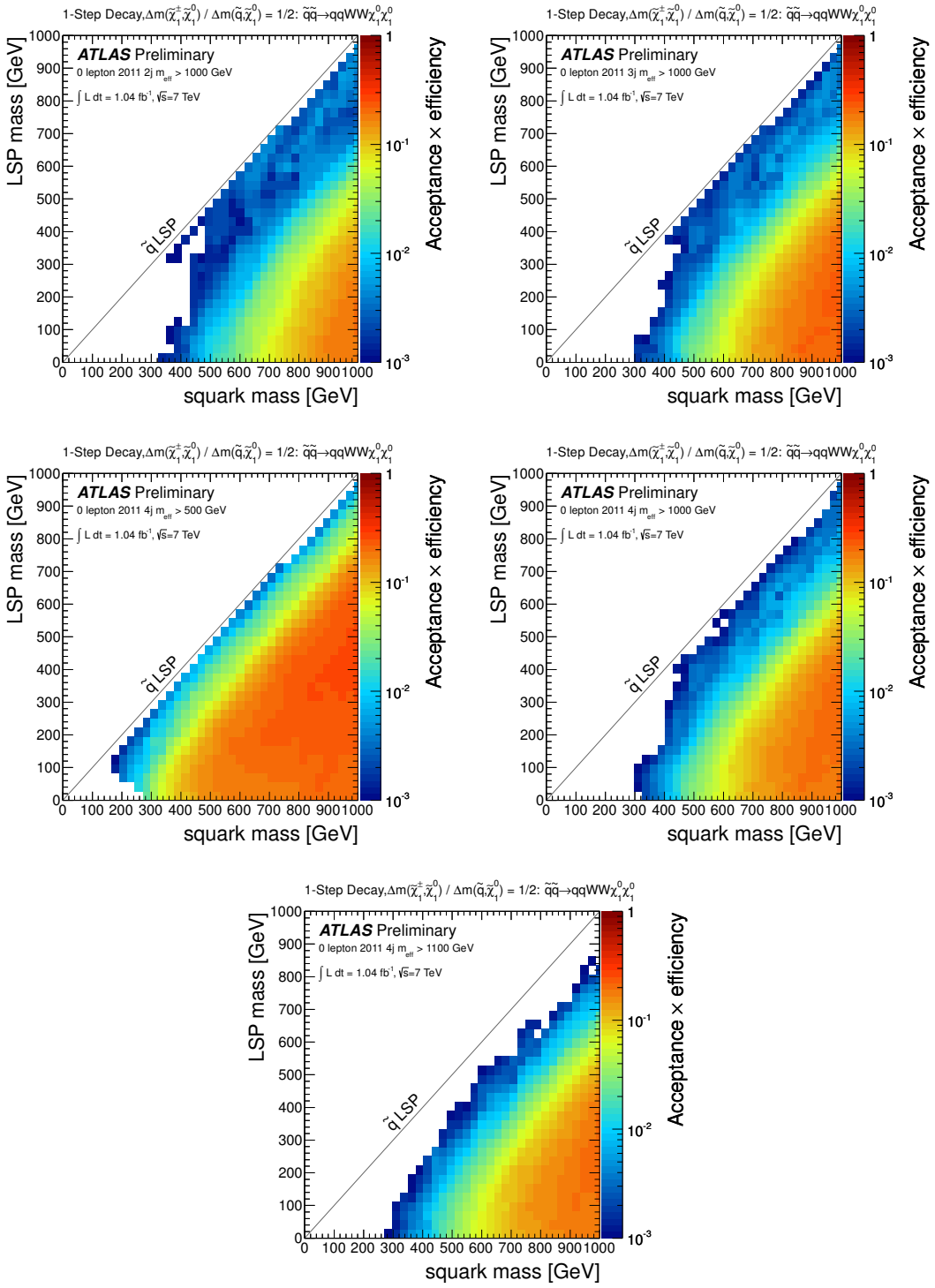


Figure 12: Acceptance times efficiency ($A \times \varepsilon$), defined as the fraction of signal events passing full event selection in the $\tilde{q} - \tilde{\chi}_1^0$ mass plane for one-step squark decays $\tilde{q} \to q\tilde{\chi}_1^{\pm} \to q\, W^{\pm} \tilde{\chi}_1^0$ with $x = 1/2$ for each of the five signal selections. Points shown in white have less than 0.1% of events accepted.

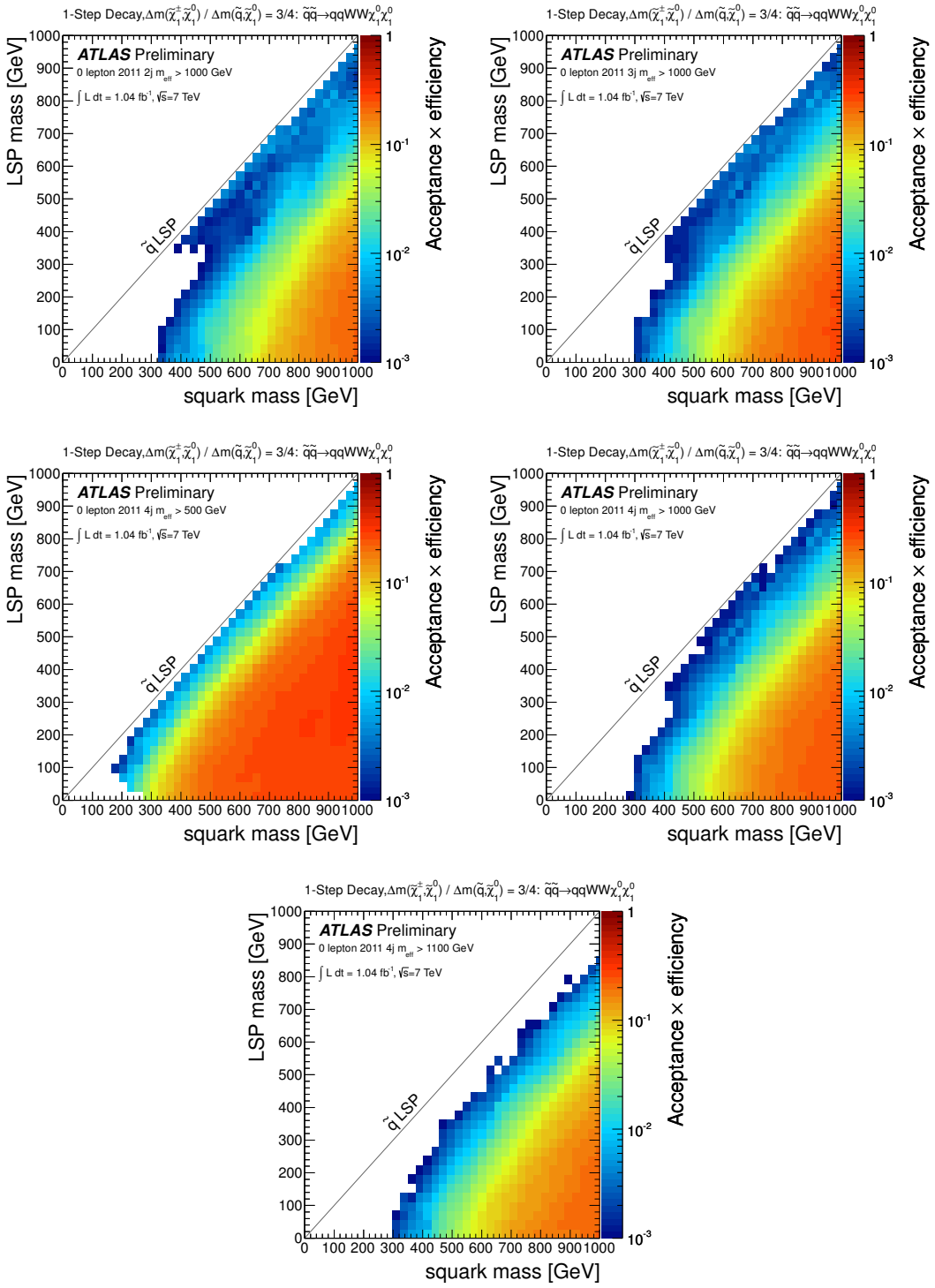


Figure 13: Acceptance times efficiency ($A \times \varepsilon$), defined as the fraction of signal events passing full event selection in the $\tilde{q}-\tilde{\chi}_1^0$ mass plane for one-step squark decays $\tilde{q} \to q\tilde{\chi}_1^{\pm} \to q\,W^{\pm}\tilde{\chi}_1^0$ with $x = 3/4$ for each of the five signal selections. Points shown in white have less than 0.1% of events accepted.

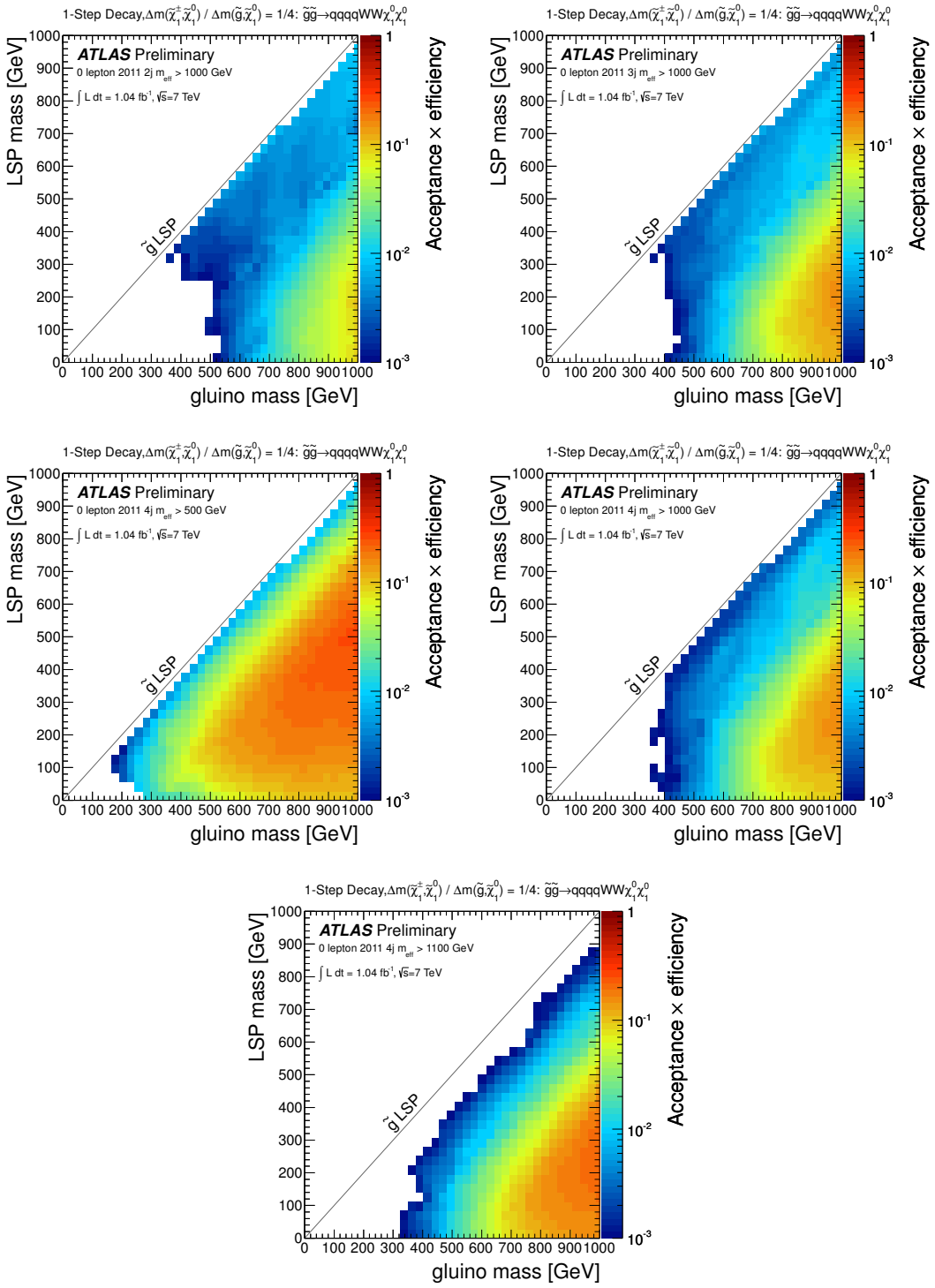


Figure 14: Acceptance times efficiency ($A \times \varepsilon$), defined as the fraction of signal events passing full event selection in the $\tilde{g} - \tilde{\chi}_1^0$ mass plane for one-step gluino decays $\tilde{g} \to q\bar{q}\tilde{\chi}_1^{\pm} \to q\bar{q}\, W^{\pm}\tilde{\chi}_1^0$ with $x = 1/4$ for each of the five signal selections. Points shown in white have less than 0.1% of events accepted.

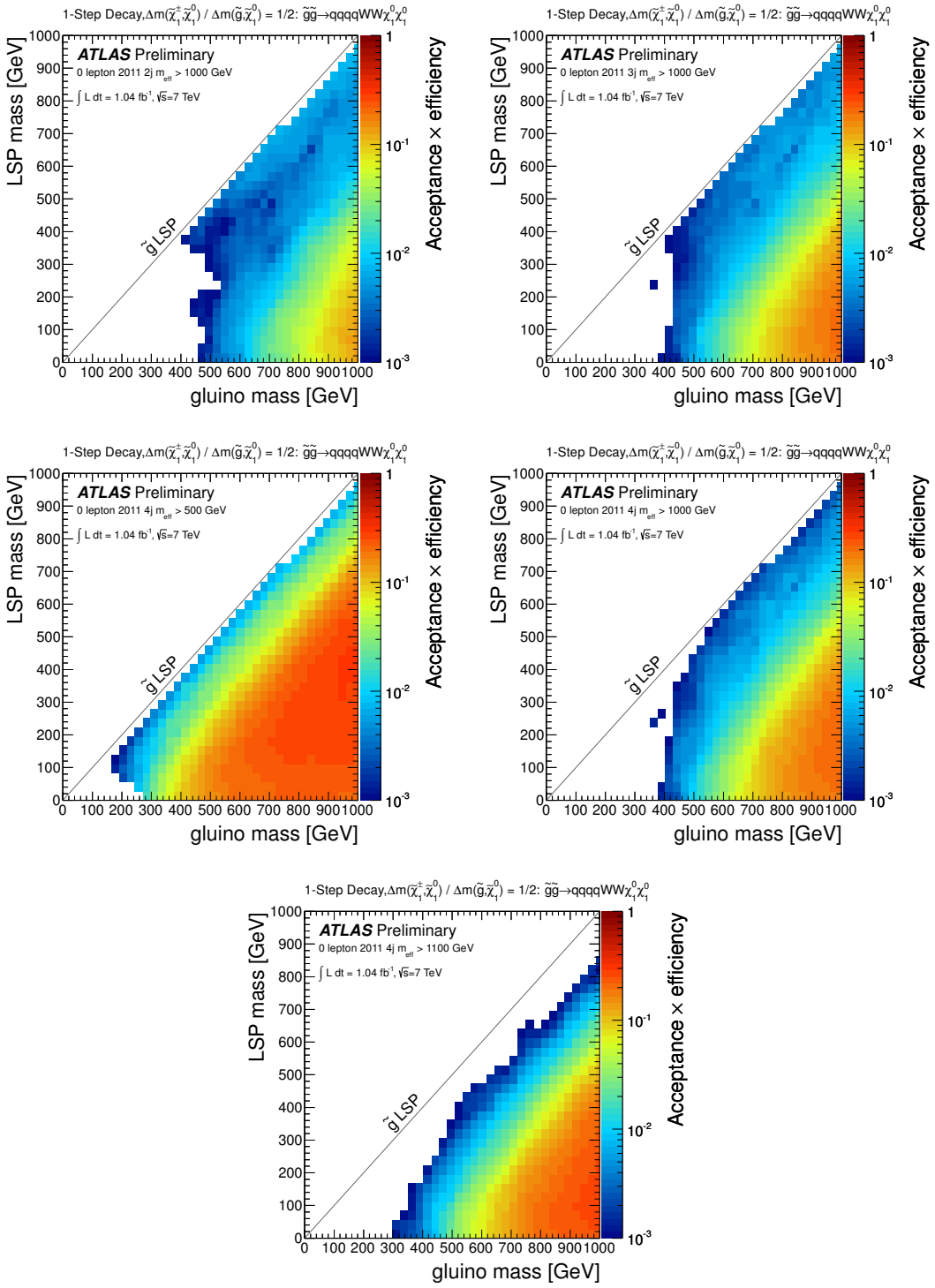


Figure 15: Acceptance times efficiency ($A \times \varepsilon$), defined as the fraction of signal events passing full event selection in the $\tilde{g} - \tilde{\chi}_1^0$ mass plane for one-step gluino decays $\tilde{g} \to q\bar{q}\tilde{\chi}_1^{\pm} \to q\bar{q}\, W^{\pm}\tilde{\chi}_1^0$ with $x = 1/2$ for each of the five signal selections. Points shown in white have less than 0.1% of events accepted.

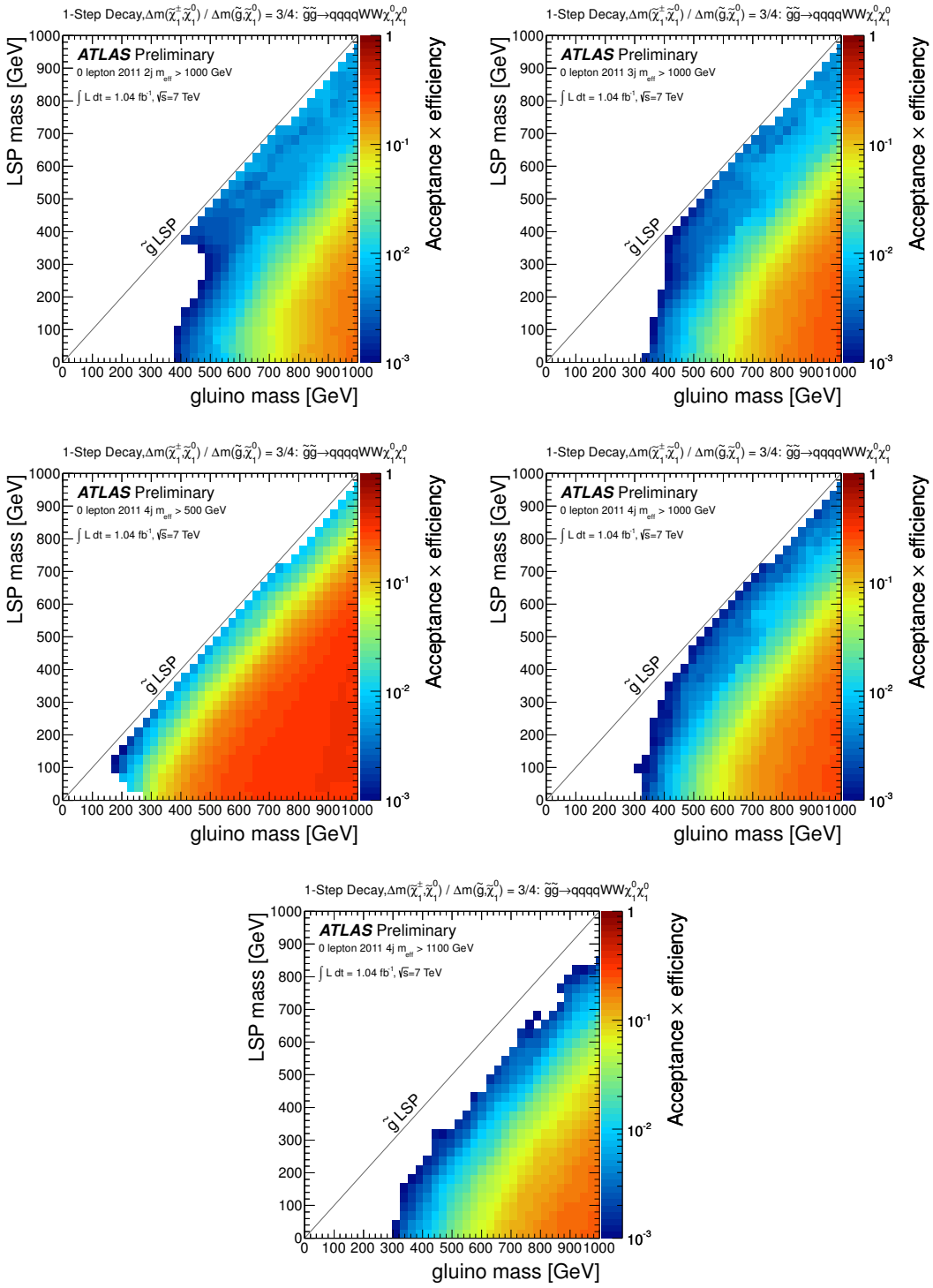


Figure 16: Acceptance times efficiency ($A \times \varepsilon$), defined as the fraction of signal events passing full event selection in the $\tilde{g} - \tilde{\chi}_1^0$ mass plane for one-step gluino decays $\tilde{g} \to q\bar{q}\tilde{\chi}_1^{\pm} \to q\bar{q}\, W^{\pm}\tilde{\chi}_1^0$ with $x = 3/4$ for each of the five signal selections. Points shown in white have less than 0.1% of events accepted.

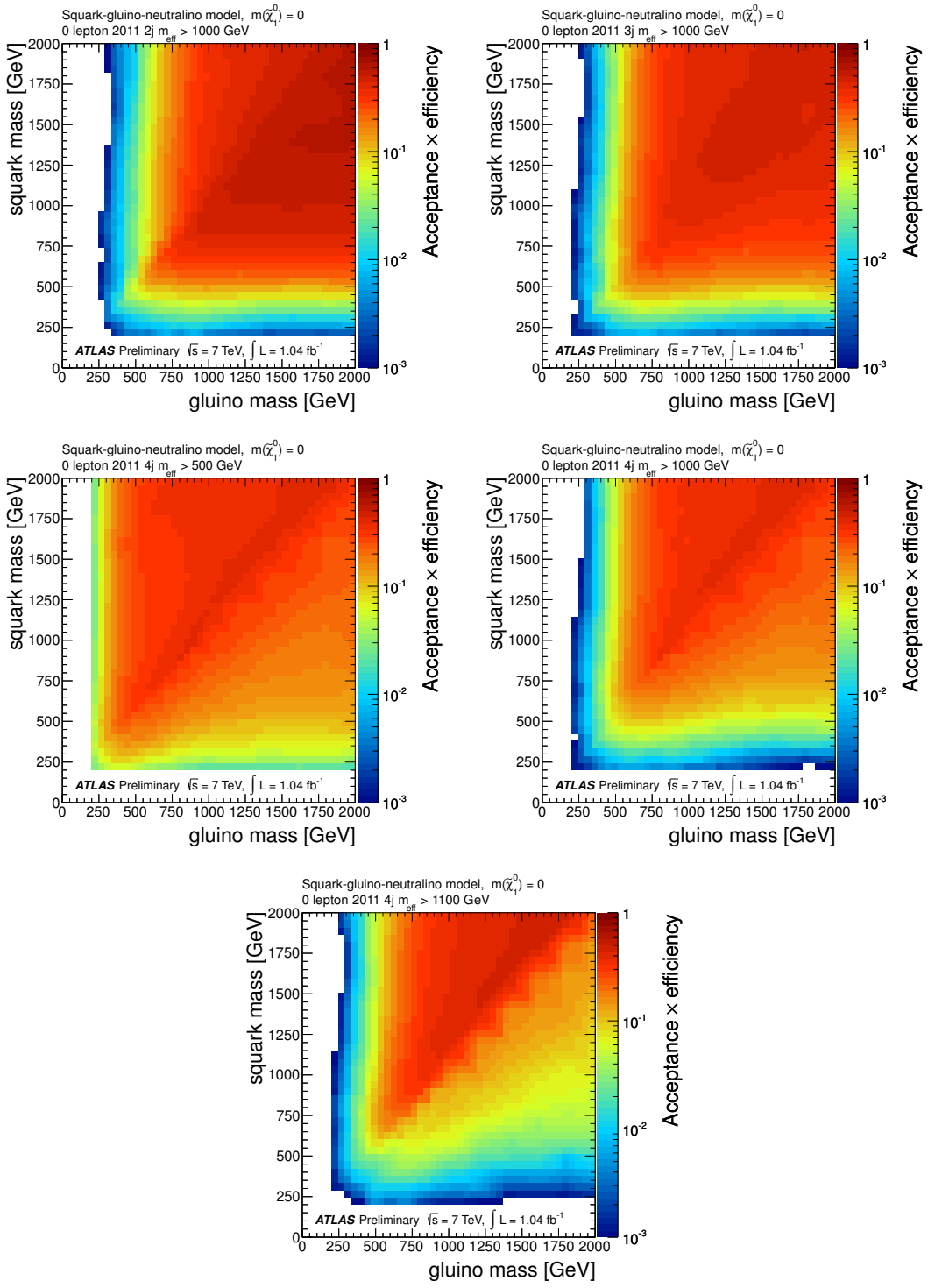


Figure 17: Acceptance times efficiency ($A \times \varepsilon$), defined as the fraction of signal events passing full event selection in the $\tilde{q} - \tilde{g}$ mass plane with massless LSP's for each of the five signal selections. Points shown in white have less than 0.1% of events accepted.

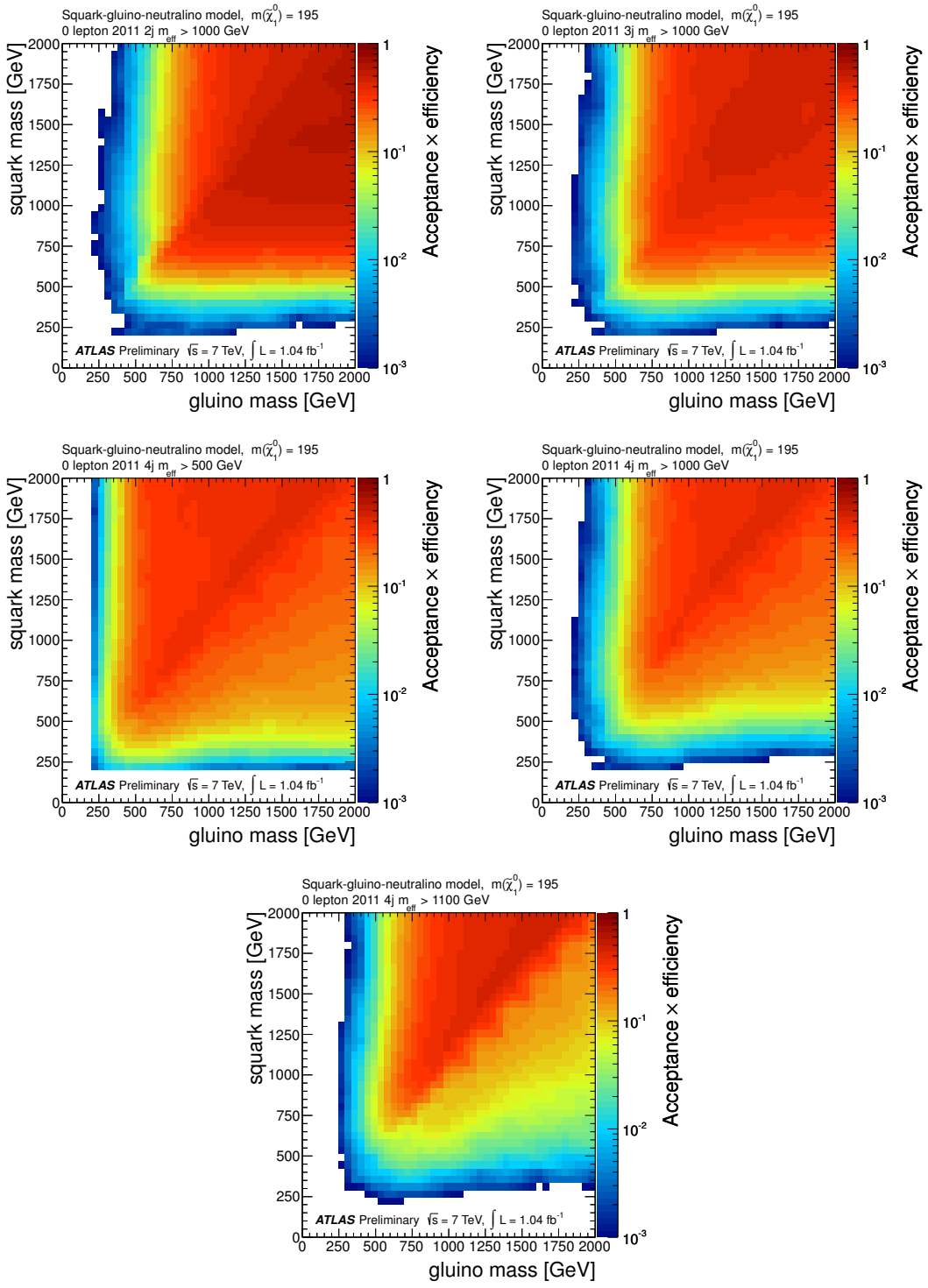


Figure 18: Acceptance times efficiency ($A \times \varepsilon$), defined as the fraction of signal events passing full event selection in the $\tilde{q} - \tilde{g}$ mass plane with 195 GeV LSP's for each of the five signal selections. Points shown in white have less than 0.1% of events accepted.

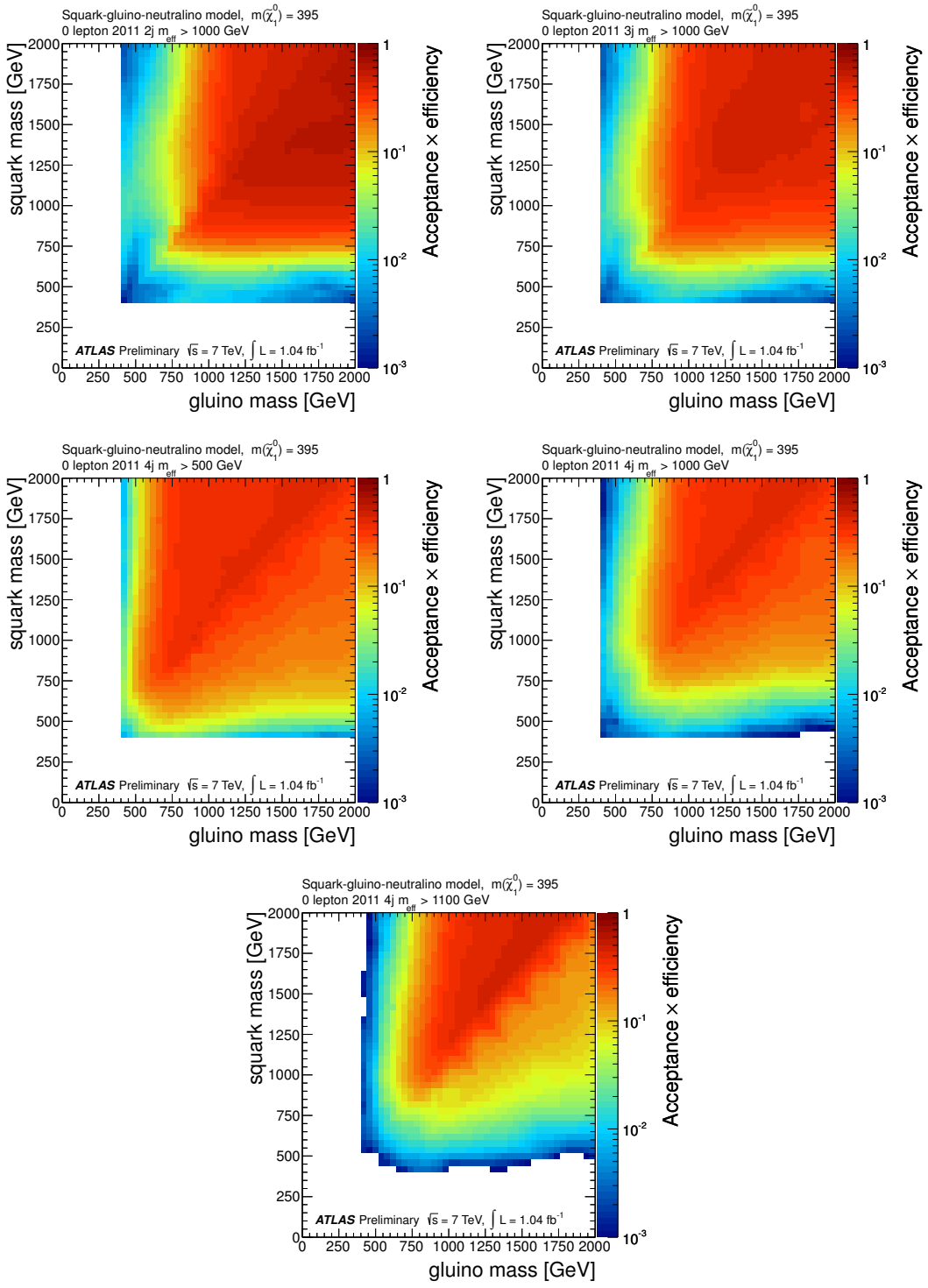


Figure 19: Acceptance times efficiency ($A \times \varepsilon$), defined as the fraction of signal events passing full event selection in the $\tilde{q} - \tilde{g}$ mass plane with 395 GeV LSP's for each of the five signal selections. Points shown in white have less than 0.1% of events accepted.

# B Additional limit plots

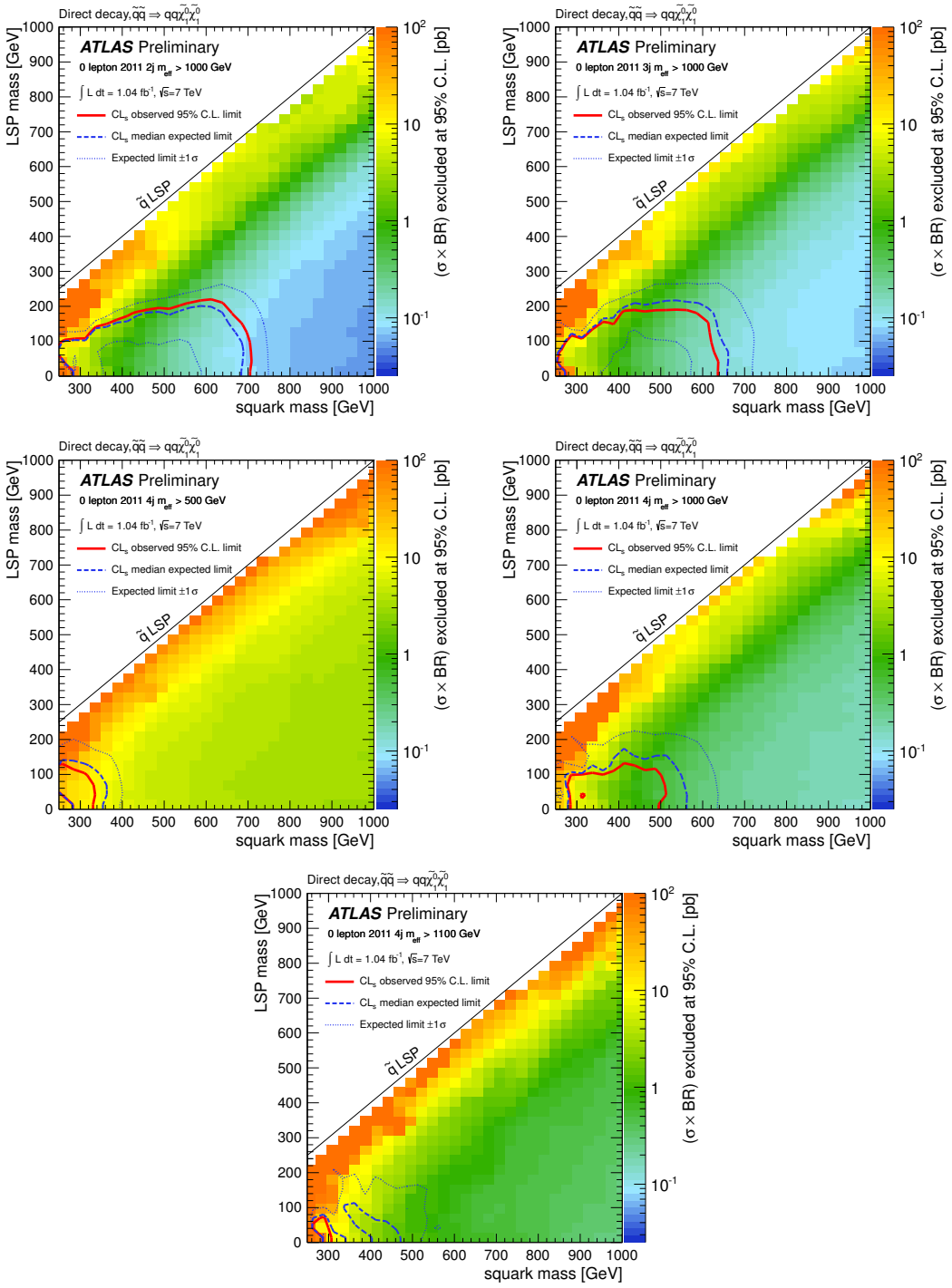


Figure 20: Exclusion limits in the $\tilde{q} - \tilde{\chi}_1^0$ mass plane for direct squark decays $\tilde{q} \rightarrow q\tilde{\chi}_1^0$ for each of the five signal selections. The colour scale shows the 95% C.L. upper limit on the production cross section.

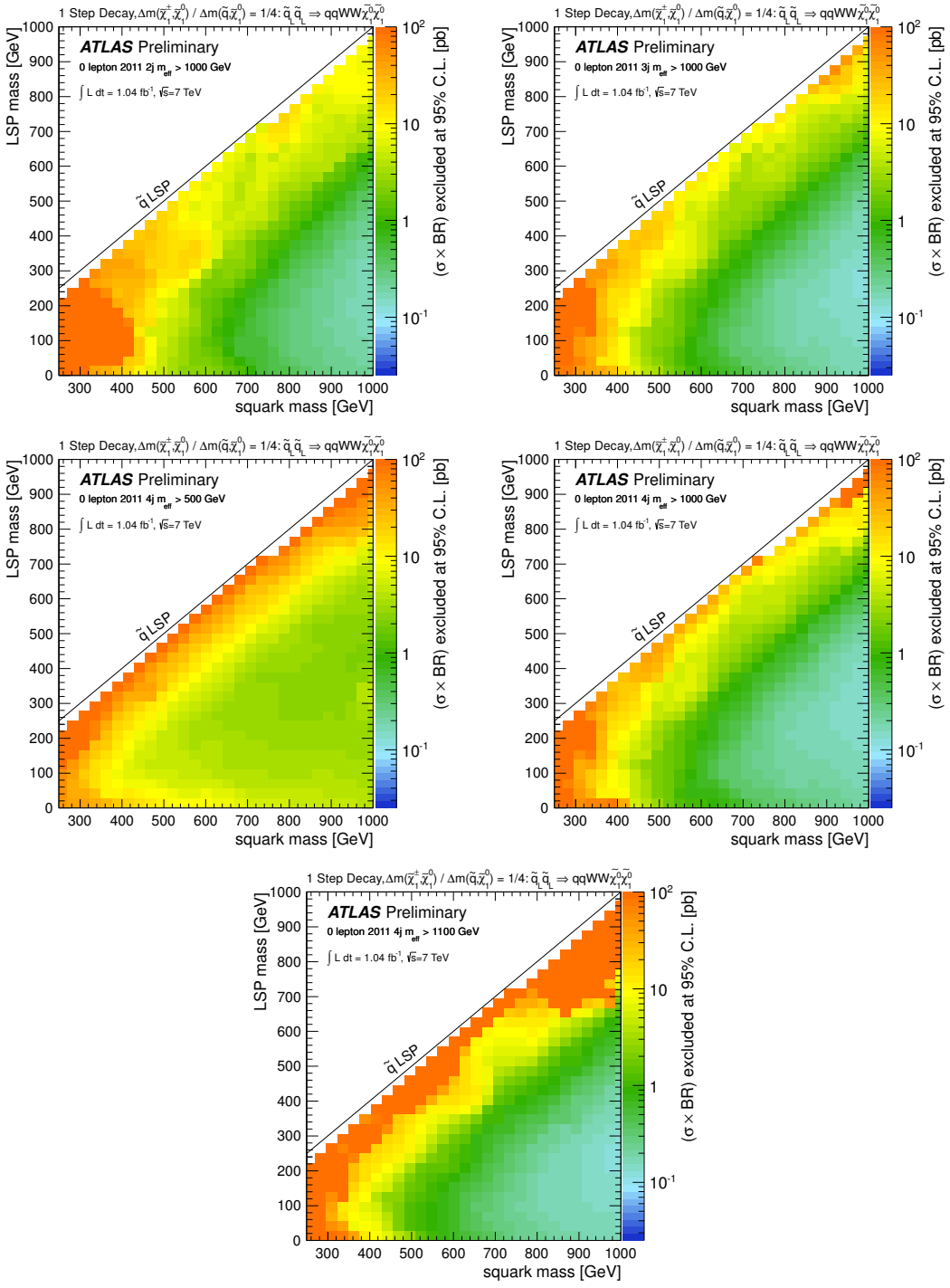


Figure 21: Exclusion limits in the $\tilde{q} - \tilde{\chi}_1^0$ mass plane for one-step squark decays $\tilde{q} \to q\tilde{\chi}_1^{\pm} \to q\,W^{\pm}\tilde{\chi}_1^0$ with $x = 1/4$ for each of the five signal selections. Only left-handed squarks are considered, effectively halving the cross section. The nominal cross sections are too low for any model points to be excluded at 95% C.L., hence no limit contours are drawn. The colour scale shows the 95% C.L. upper limit on the production cross section.

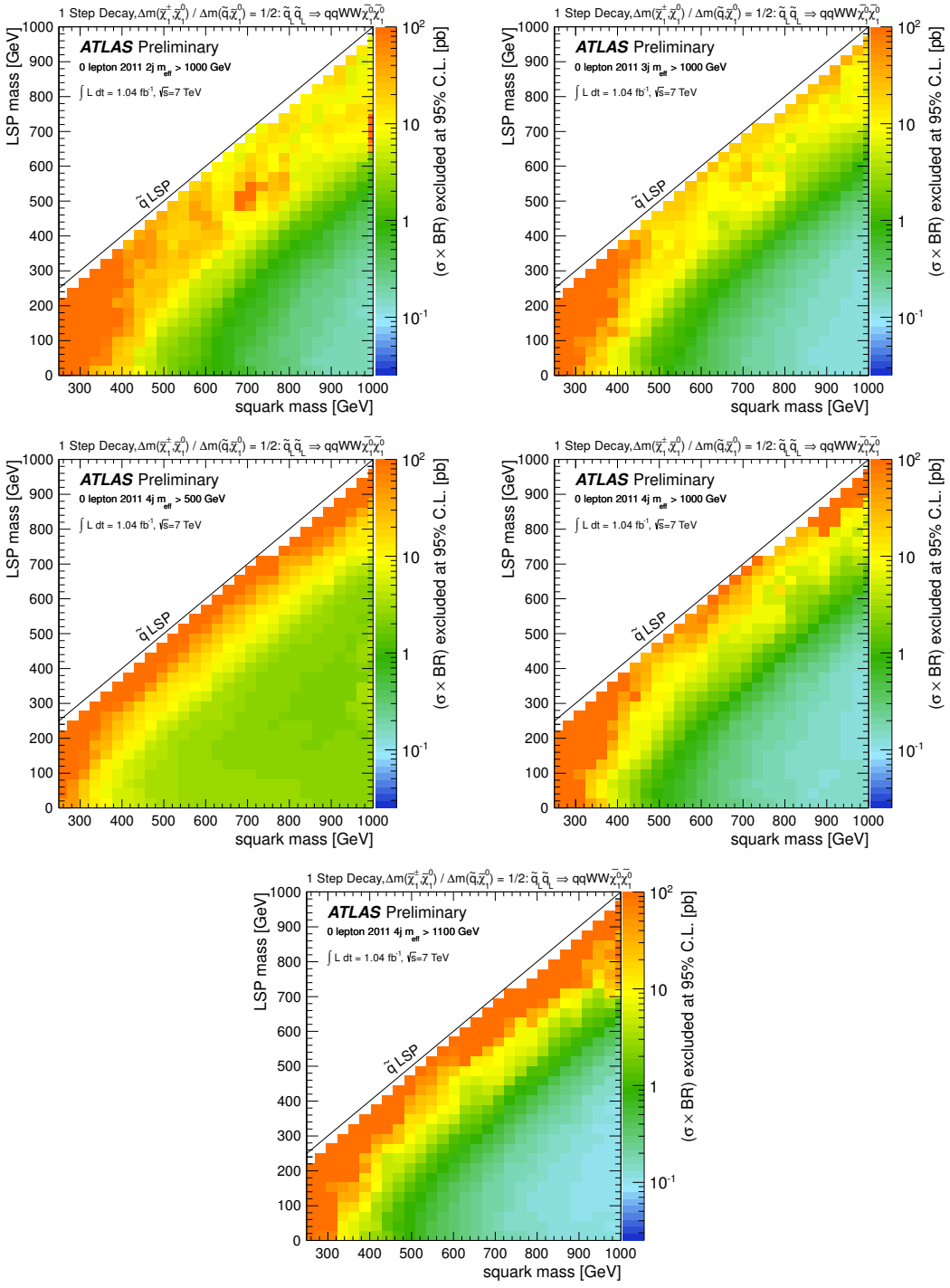


Figure 22: Exclusion limits in the $\tilde{q} - \tilde{\chi}_1^0$ mass plane for one-step squark decays $\tilde{q} \to q\tilde{\chi}_1^{\pm} \to q\,W^{\pm}\tilde{\chi}_1^0$ with $x = 1/2$ for each of the five signal selections. Only left-handed squarks are considered, effectively halving the cross section. The nominal cross sections are too low for any model points to be excluded at 95% C.L., hence no limit contours are drawn. The colour scale shows the 95% C.L. upper limit on the production cross section.

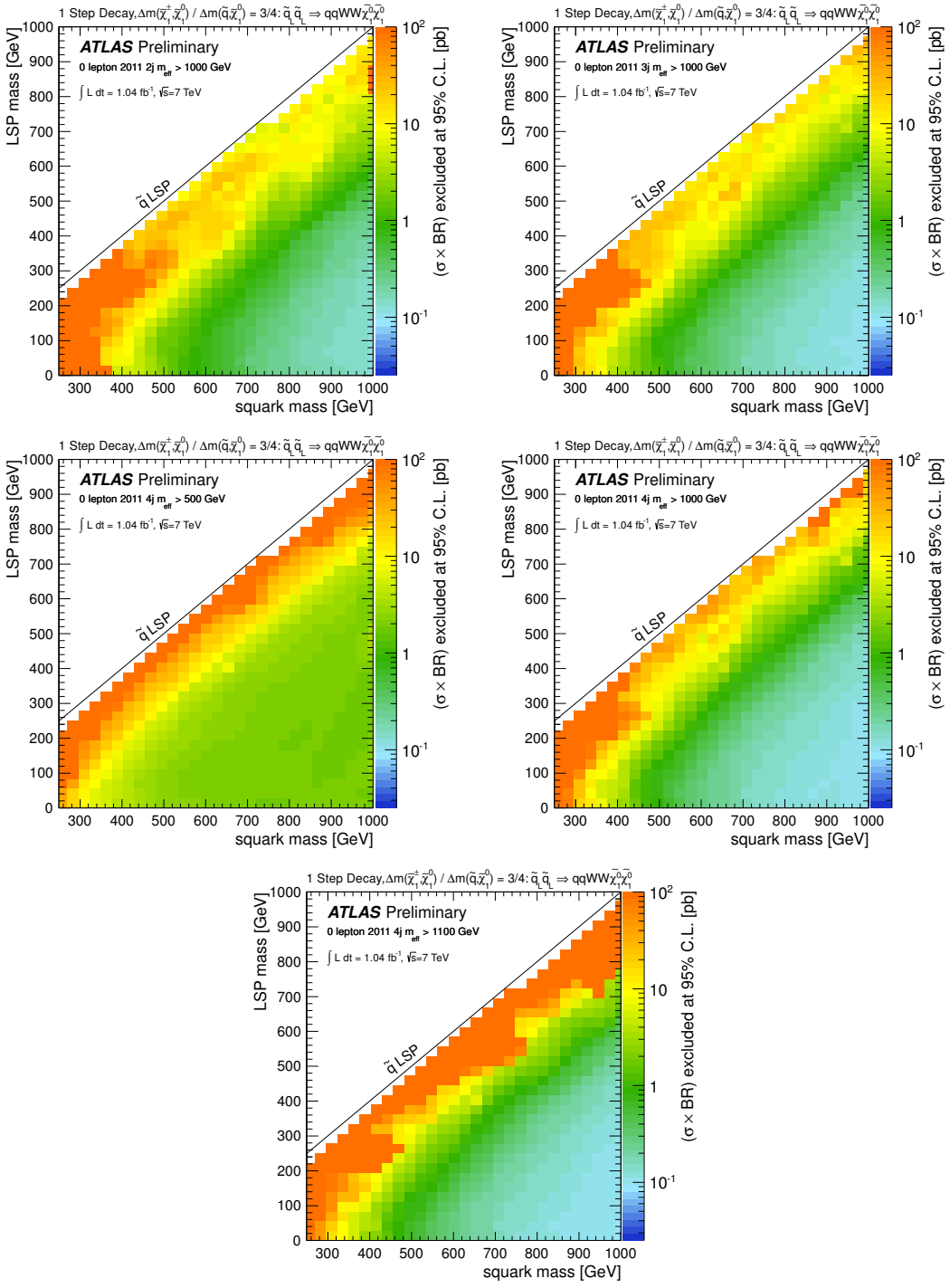


Figure 23: Exclusion limits in the $\tilde{q} - \tilde{\chi}_1^0$ mass plane for one-step squark decays $\tilde{q} \to q\tilde{\chi}_1^{\pm} \to q\,W^{\pm}\tilde{\chi}_1^0$ with $x = 3/4$ for each of the five signal selections. Only left-handed squarks are considered, effectively halving the cross section. The nominal cross sections are too low for any model points to be excluded at 95% C.L., hence no limit contours are drawn. The colour scale shows the 95% C.L. upper limit on the production cross section.

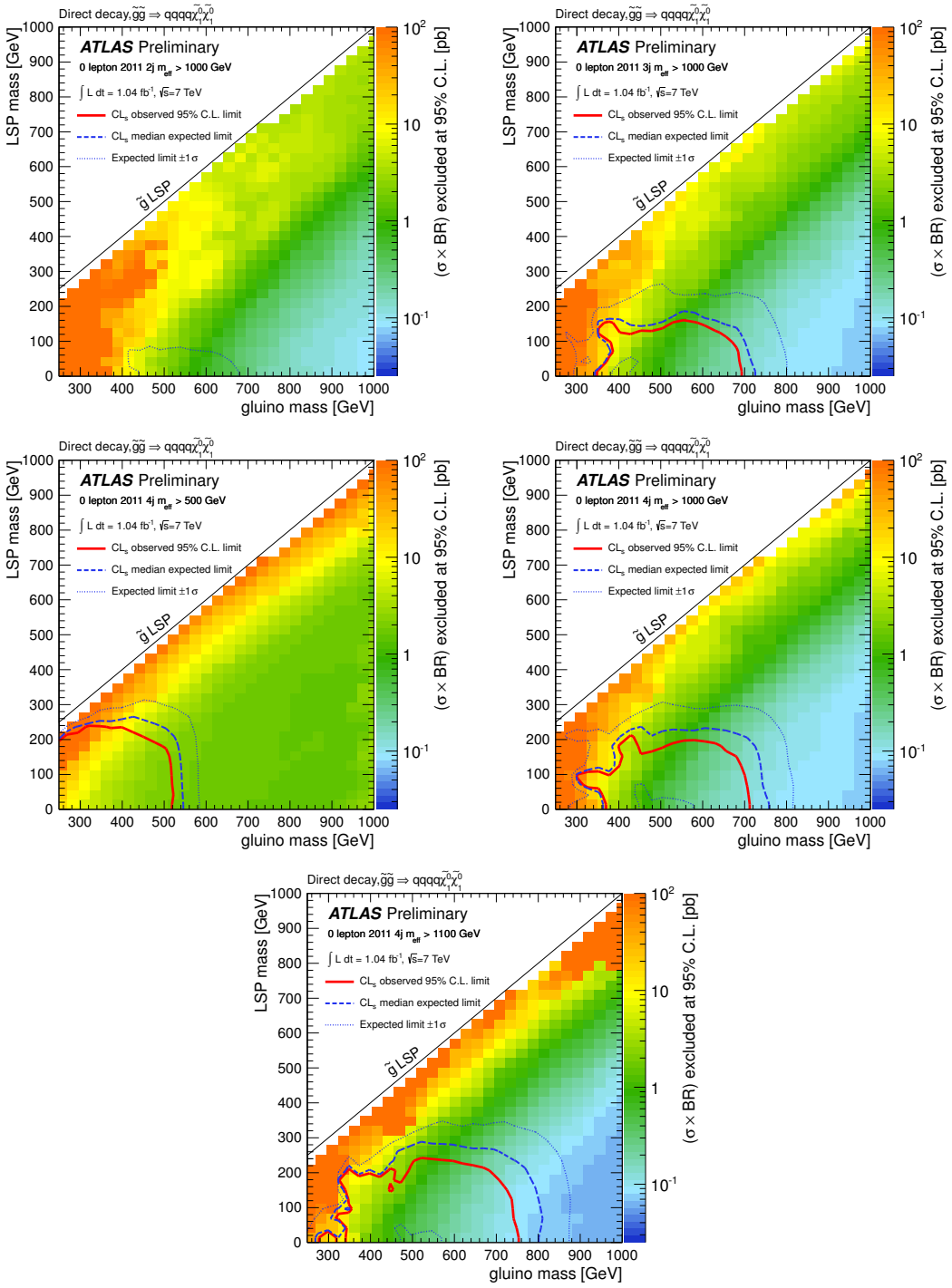


Figure 24: Exclusion limits in the $\tilde{g} - \tilde{\chi}_1^0$ mass plane for direct gluino decays $\tilde{g} \to q\bar{q}\tilde{\chi}_1^0$ for each of the five signal selections. The colour scale shows the 95% C.L. upper limit on the production cross section.

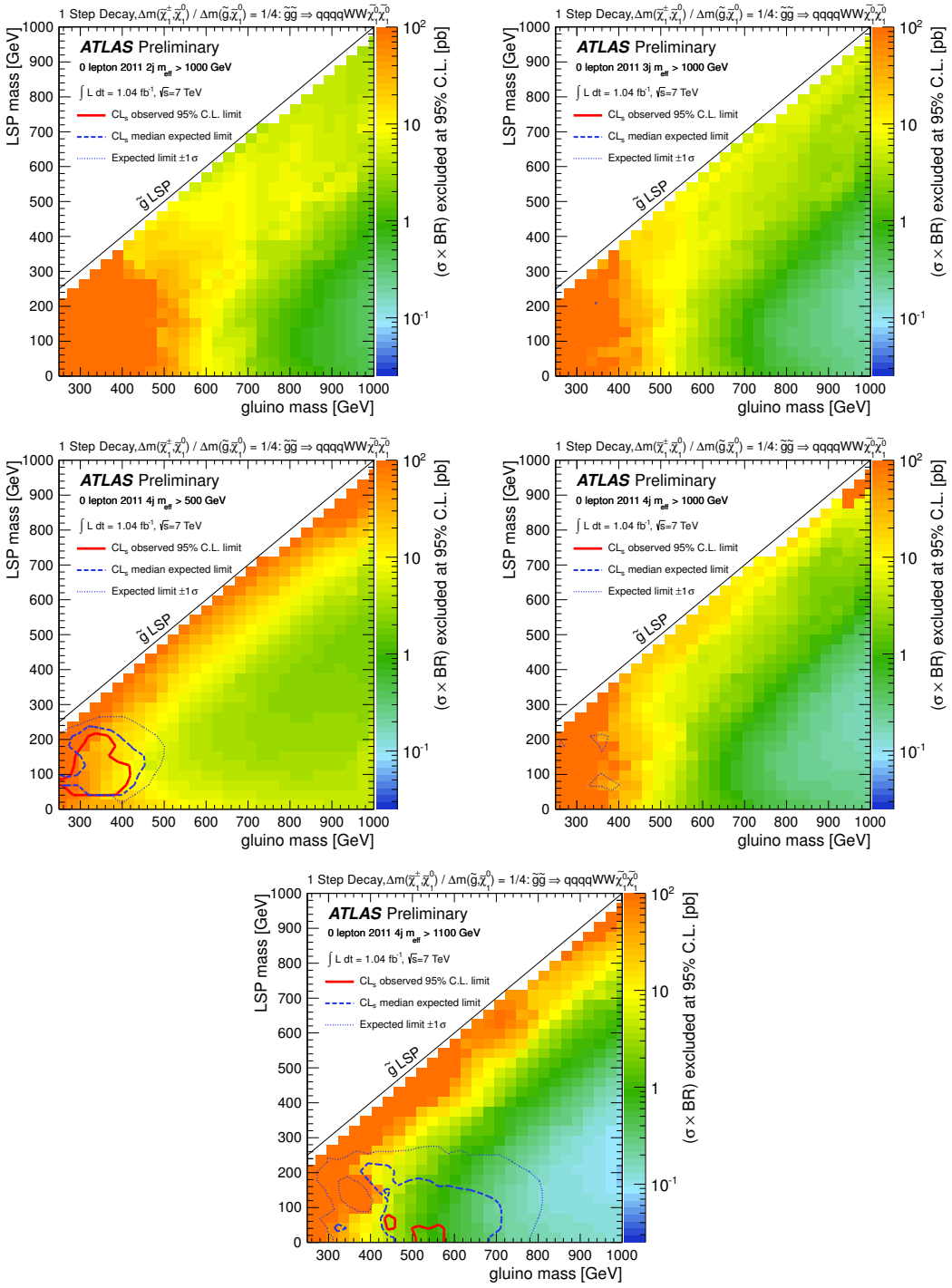


Figure 25: Exclusion limits in the $\tilde{g} - \tilde{\chi}_1^0$ mass plane for one-step gluino decays $\tilde{g} \to q\bar{q}\tilde{\chi}_1^{\pm} \to q\bar{q}\, W^{\pm}\tilde{\chi}_1^0$ with $x = 1/4$ for each of the five signal selections. The colour scale shows the 95% C.L. upper limit on the production cross section.

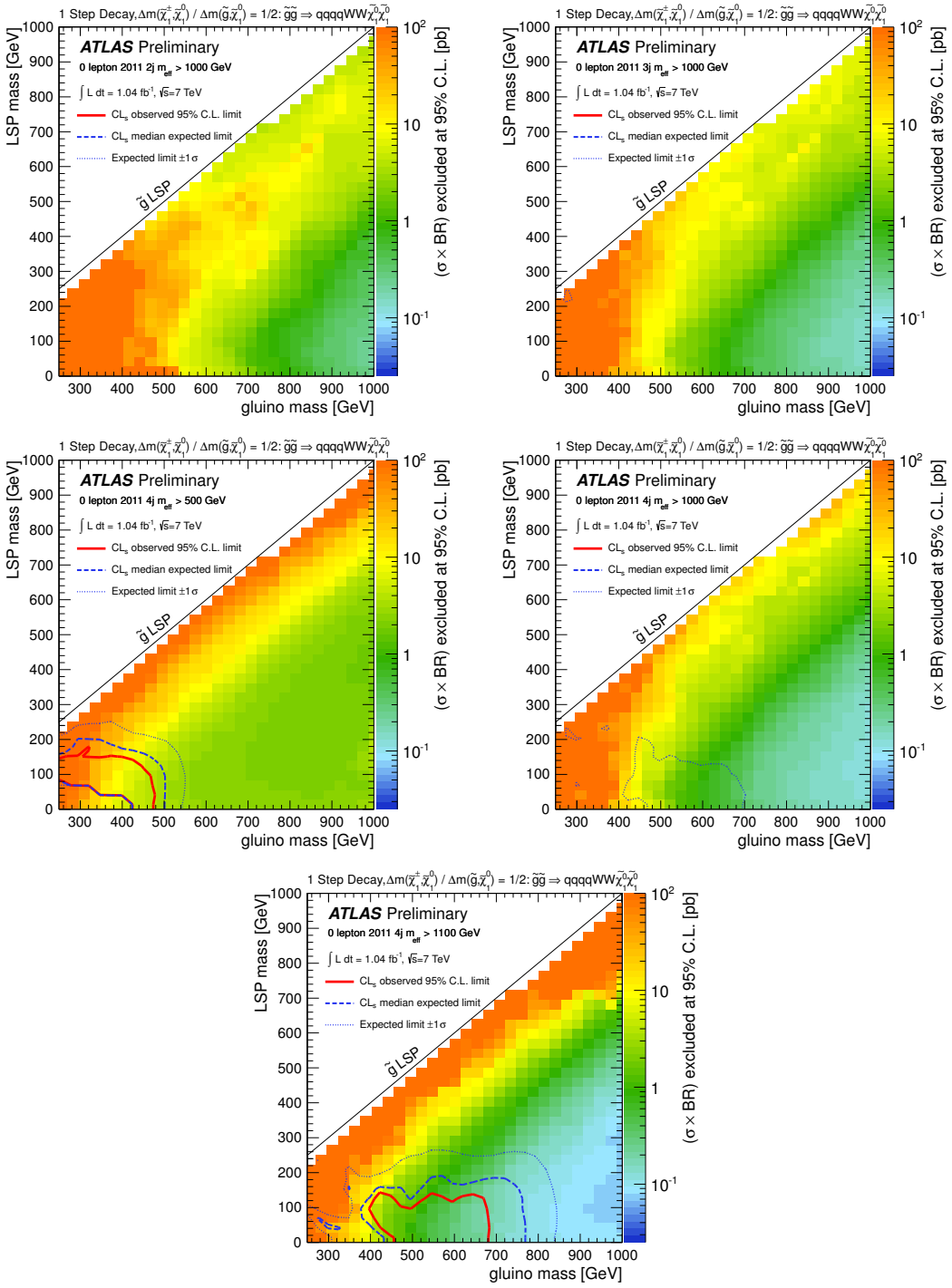


Figure 26: Exclusion limits in the $\tilde{g} - \tilde{\chi}_1^0$ mass plane for one-step gluino decays $\tilde{g} \to q\bar{q}\tilde{\chi}_1^{\pm} \to q\bar{q}\, W^{\pm}\tilde{\chi}_1^0$ with $x = 1/2$ for each of the five signal selections. The colour scale shows the 95% C.L. upper limit on the production cross section.

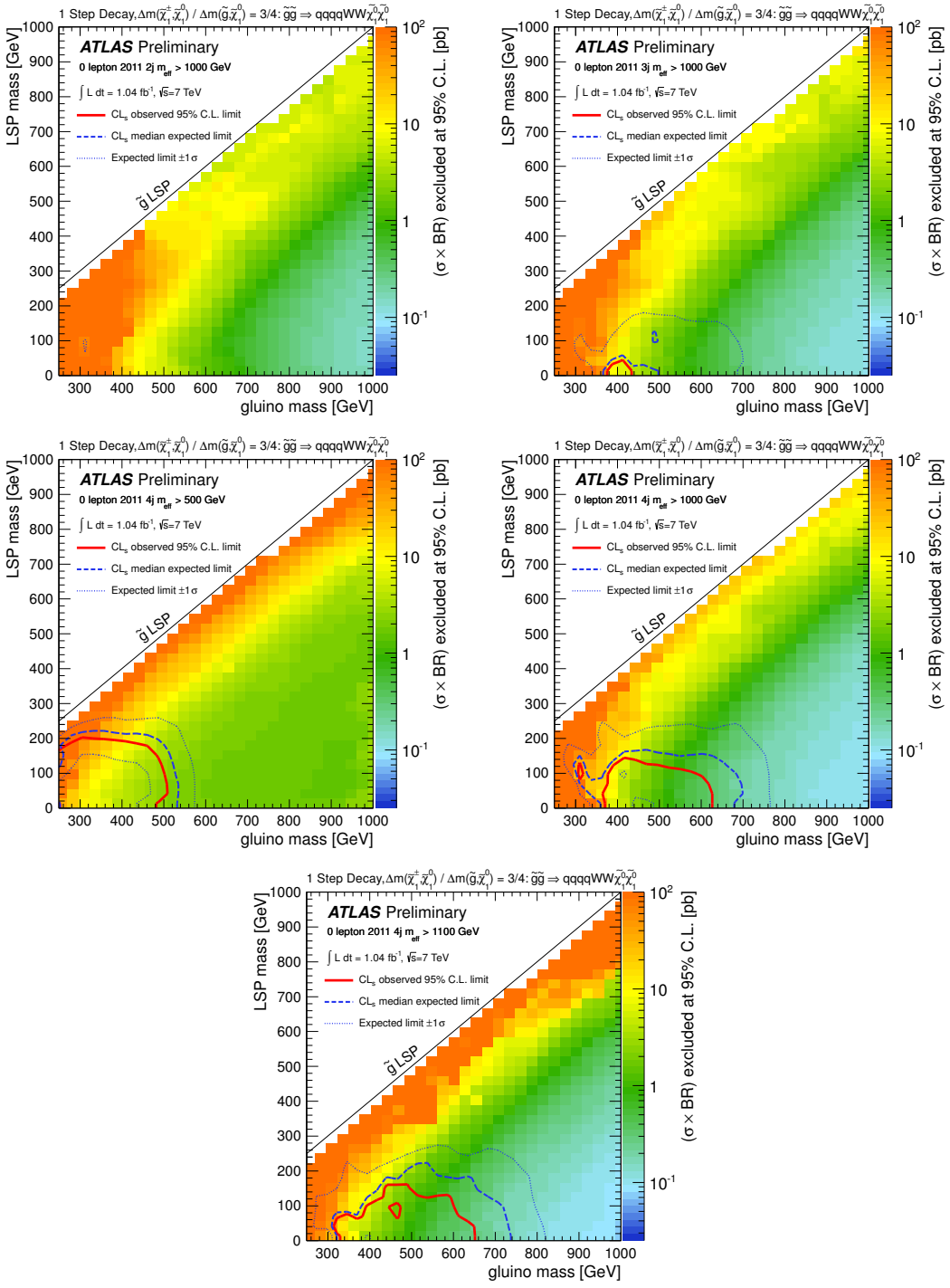


Figure 27: Exclusion limits in the $\tilde{g} - \tilde{\chi}_1^0$ mass plane for one-step gluino decays $\tilde{g} \to q\bar{q}\tilde{\chi}_1^{\pm} \to q\bar{q}\, W^{\pm}\tilde{\chi}_1^0$ with $x = 3/4$ for each of the five signal selections. The colour scale shows the 95% C.L. upper limit on the production cross section.

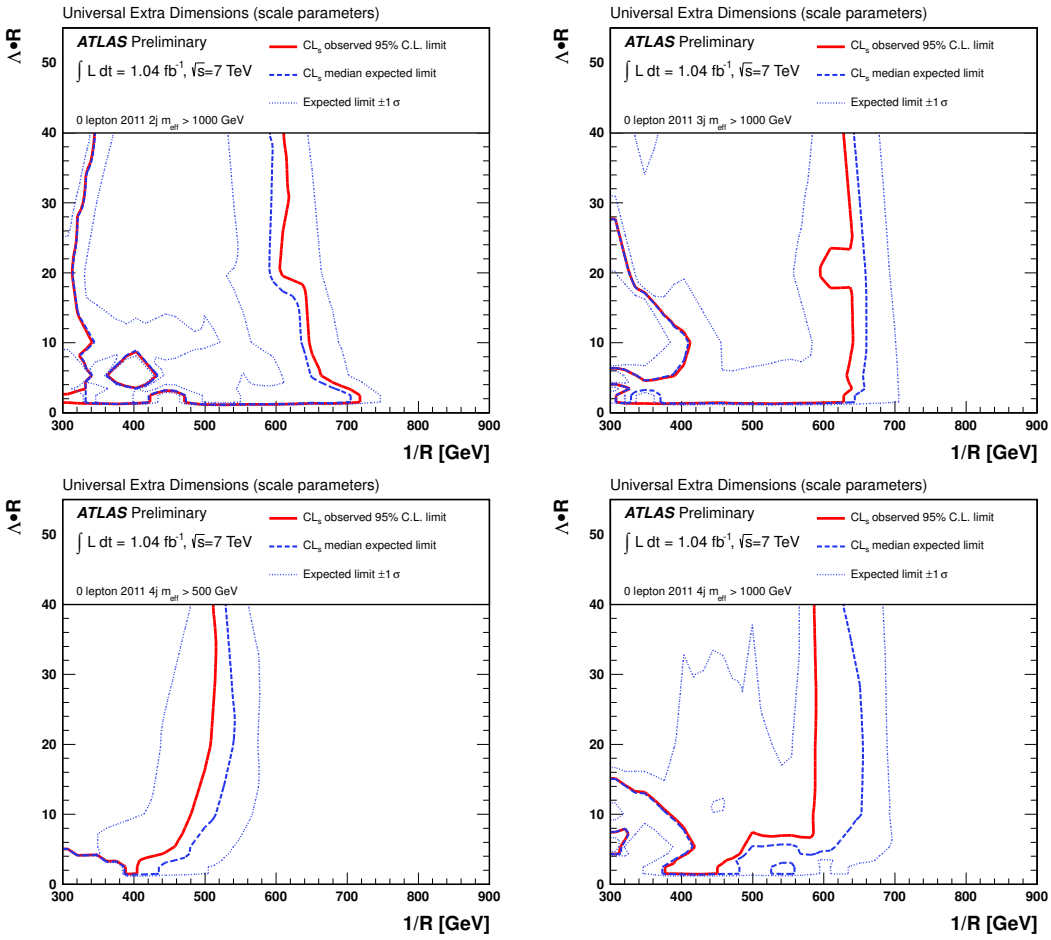


Figure 28: Exclusion limits in the Universal Extra Dimensions model space, in terms of the scale of the extra dimension ($R^{-1}$) and the compression scale ($\Lambda \cdot R$). The high-mass signal region does not contribute to the limit, and is not shown.

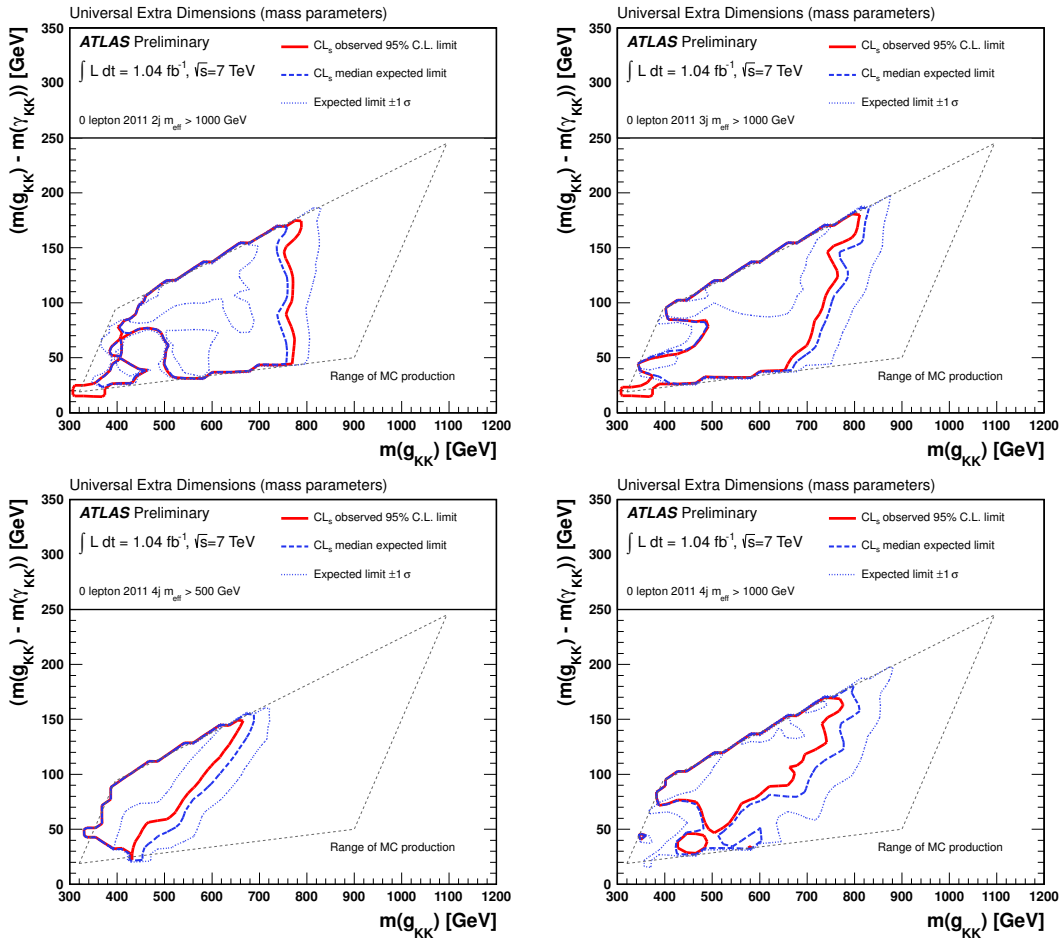


Figure 29: Exclusion limits in the Universal Extra Dimensions model space, in terms of the masses of the Kaluza-Klein gluon $g_{\mathrm{KK}}$ and the Kaluza-Klein photon $\gamma_{\mathrm{KK}}$ (LKP). The high-mass signal region does not contribute to the limit, and is not shown.

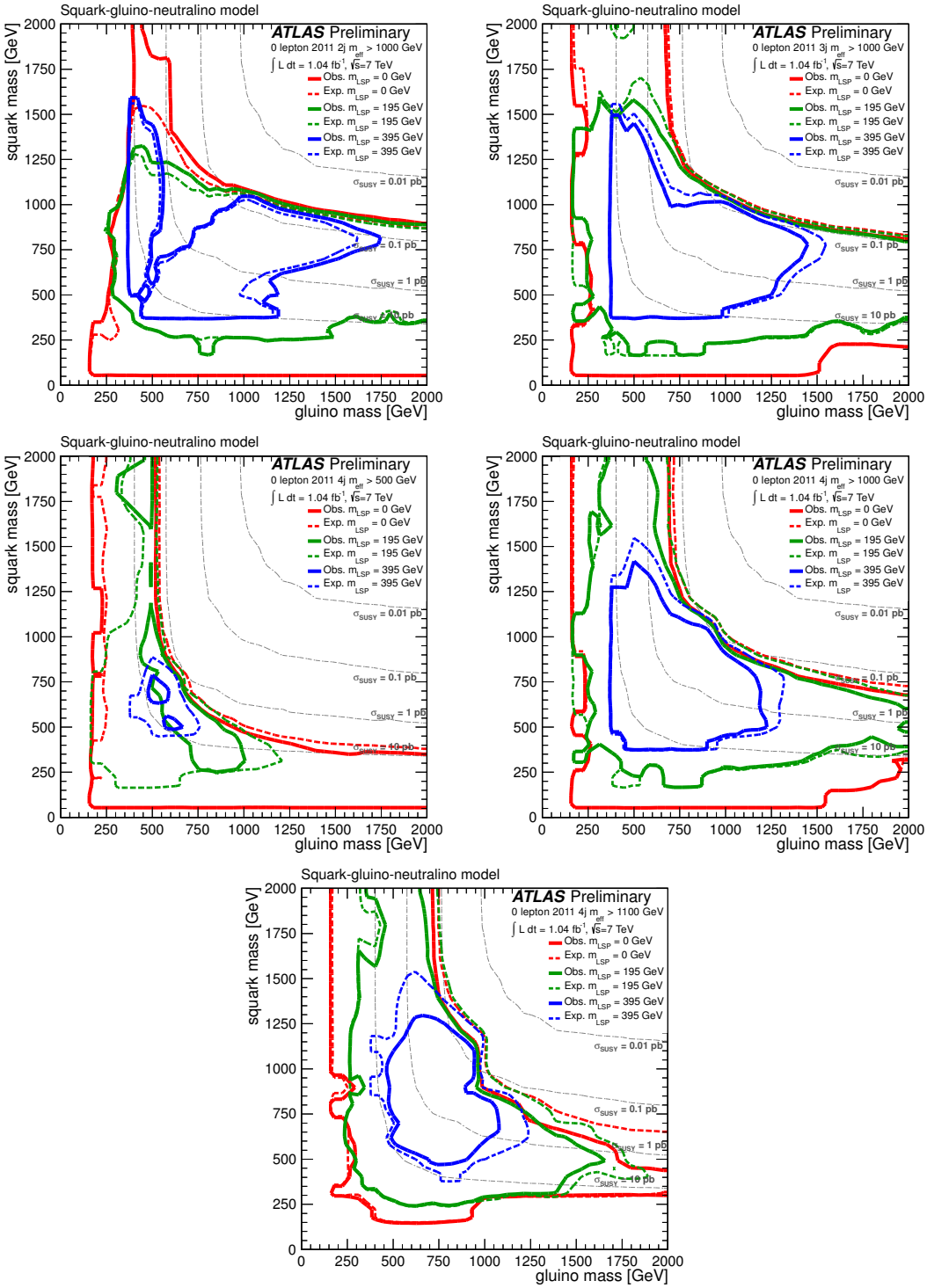


Figure 30: Exclusion limits in the $\tilde{g} - \tilde{q}$ mass plane with $m_{\text{LSP}} = 0, 195, 395$ GeV for each of the five signal selections.